STANFORD UNIVERSITY
ENGINEERING IN MEDICINE AND BIOLOGY

DIRECT DETERMINATION OF DISTENSIBILITY OF THE LEFT VENTRICLE OF THE HEART UNDER IN VIVO CONDITIONS

ENGINEER THESIS

BY

WILLIAM J. ASTLEFORD

BIOMECHANICS LABORATORY

DEPARTMENT OF AERONAUTICS AND ASTRONAUTICS

MARCH 1969

This work was carried out at the Ames Research Center of NASA with the support of NASA Grant NGR 05-020-223

SUDAAR NO. 372

Department of Aeronautics and Astronautics
Stanford University
Stanford, California

DIRECT DETERMINATION OF DISTENSIBILITY OF THE LEFT VENTRICLE OF THE HEART UNDER IN VIVO CONDITIONS

Engineer Thesis

by

William J. Astleford

SUDAAR NO. 372
March 1969

This work was carried out at the Ames Research Center of NASA
with the support of NASA Grant NGR 05-020-223

DIRECT DETERMINATION OF DISTENSIBILITY OF THE LEFT VENTRICLE OF THE HEART UNDER IN VIVO CONDITIONS

A THESIS

SUBMITTED TO THE

DEPARTMENT OF AERONAUTICS AND ASTRONAUTICS

AND THE COMMITTEE ON THE GRADUATE DIVISION

OF STANFORD UNIVERSITY

IN PARTIAL FULFILLMENT OF THE REQUIREMENTS

FOR THE DEGREE OF

ENGINEER

By

William James Astleford

December, 1968

ACKNOWLEDGMENTS

I wish to express my appreciation to my thesis advisor, Professor Max Anliker, for giving me the opportunity to participate in a new and rapidly expanding technology — the application of engineering to the medical sciences. His guidance and encouragement were invaluable aids during the research for this thesis. I would like to thank Dr. Eric Ogden of the Life Sciences Division of NASA Ames Research Center for his medical counseling, Professors C. C. Chao and I-Dee Chang for their constructive comments on the theoretical aspects of this research and Mrs. Jane Fajardo for her speedy and efficient typing of the final manuscript.

This work was carried out at Ames Research Center of NASA with the support of NASA Grant NGR 05-020-223.

TABLE OF CONTENTS

LIST OF FIGURES

LIST OF FIGURES (Continued)

LIST OF SYMBOLS

A_1, A_2	amplitude of the galvanometer deflections corresponding to the first and second heart sounds, mm
E	effective Young's modulus, dynes/cm^2
f	perturbation frequency, Hz
f_c	filter band-pass center frequency, Hz
f_n	heart rate, Hz
$F(f, f_c)$	filter characteristic
Δp	pressure response to volumetric perturbation, mm Hg or dynes/cm^2
r, θ, ϕ	spherical coordinates
r_e, r_i	external and internal spherical shell radii, cm
T	period of sound spectrum component resulting from the filtering process, sec
u_i	displacement components in the coordinate directions, cm
V_{io}, V_i	unperturbed and perturbed ventricular volume, cm^3
ΔV	volumetric perturbation, cm^3 or mm^3
V_w	ventricular wall volume, cm^3
W_{HEART}	heart weight, gm
ϵ_{ij}	elements of the strain tensor, cm/cm
λ, μ	Lamé constants
ρ_w	density of the ventricular wall, gm/cm^3
σ_{ij}	elements of the stress tensor, dynes/cm^2
Φ	hydrostatic pressure, dynes/cm^2

∇	del operator
∇^2	Laplacian operator
δ_{ij}	Kronecker delta
$\ddot{(\ )}$	second partial derivative with respect to time
$(\ )_{i,j}$	partial derivative of the i^{th} component of a vector with respect to the j^{th} coordinate direction
$\overline{(\ )}$	vector quantity

1. INTRODUCTION

The physical condition of the mammalian heart can be assessed in part through its acoustical properties which reflect the geometric features of the heart and the mechanical properties of the myocardium. In a qualitative sense this fact has long been utilized in medicine in the form of auscultation and phonocardiography. While a qualitative evaluation of the heart sounds has proven helpful in detecting pathologic conditions of the heart, a quantitative analysis of the sounds would probably minimize some of the uncertainties in the diagnosis. For a given geometric configuration of the heart, the frequency spectra of the heart sounds should theoretically lend themselves to an indirect quantitative determination of the mechanical properties of the myocardium without requiring the penetration of the skin. Such a quantitative determination is, however, only possible after a valid mathematical model has been established which relates the geometric and material parameters of the heart to its acoustical properties and its dynamic response characteristics. As part of a systematic effort to evaluate the accuracy of various possible mathematical models a number of animal experiments have been devised which should allow for a more direct determination of the mechanical behavior of the heart.

The objectives of this thesis are twofold:

1. to obtain quantitative information on the effective material properties of the in vivo canine cardiac muscle through distensibility measurements;
2. to obtain frequency spectra of intravascularly recorded heart sounds.

2. THEORETICAL CONSIDERATIONS PERTAINING TO THE DISTENSIBILITY OF THE LEFT VENTRICLE OF THE HEART

The overall distensibility of the ventricular cavity is of physiological interest because it is related to the ability of the myocardium to resist stretch. The reciprocal of distensibility is termed "stiffness" and is defined as the change in ventricular cavity pressure per unit change in cavity volume. Through the use of a geometric model of the ventricle and a mathematical model describing the mechanical behavior of the wall material, the distensibility can be related to the material properties of the cardiac muscle. The temporal relationship of the events which comprise the cardiac cycle can be found in many texts on physiology (1, 2, 3). The anatomical relationship of the canine heart and its major vessels is shown in Figure 1.

2.1 Definition of the Problem

Anatomically the left ventricle of the heart does not assume a geometric configuration that lends itself to convenient analytic description. Both papillary muscles and infoldings of the endocardial surface during systole contribute to the geometric complexity of the ventricle. Therefore, an approximation must be made regarding its shape. Some investigators have considered the left ventricle to be a hemispherically-capped cone, a cylinder or an ellipsoid of revolution. In the succeeding analysis the ventricle is assumed to behave like a thick-walled spherical shell. The assumption of a thick wall is mandatory since we know from autopsy that the effective cavity radius to wall thickness ratio is of the order two and thus is far below the range where thin shell analysis is applicable. The coordinate system to which this shell is referred is shown in Figure 2.

There is evidence, as will be shown, that the effective material properties of the myocardium vary in a dramatic fashion during each cardiac cycle. Therefore, an all-encompassing theoretical description of the dynamic response characteristics of the ventricle must allow for the dependence of the material properties on the phase of the cardiac cycle. To circumvent some of the difficulties involved in such a description we assume that the cardiac cycle can be decomposed into a series of quasi-static equilibrium states. The mechanical properties of the heart for each of these states can then be obtained by perturbing the equilibrium configuration. These perturbations are induced during a sufficiently short period of time such that changes in the instantaneous heart geometry and material properties can be neglected. It is further assumed that during the perturbation process the ventricular wall is isotropic, linearly elastic and incompressible with respect to small deformations, and that the effects of fluid inertia may be disregarded.

2.2 Governing Equations and Boundary Conditions

Expressed in Cartesian tensor notation the general equations governing small deformations of the shell wall are:

$\sigma_{ij,j} + \rho_w F_i = 0 \quad , \quad F_i = -\ddot{u}_i$	(Equations of motion)	2.2.1
$\epsilon_{ij} = \frac{1}{2}(u_{i,j} + u_{j,i})$	(Strain-displacement relation)	2.2.2
$\sigma_{ij} = \lambda \epsilon_{kk} \delta_{ij} + 2\mu \epsilon_{ij}$	(Constitutive law)	2.2.3
$\epsilon_{kk} = u_{i,i} = 0$	(Incompressibility condition)	2.2.4

where σ_{ij} , ϵ_{ij} and u_i are the components of the stress and strain tensor and the displacements in the coordinate directions, respectively. The quantities λ and μ are the Lamé constants. Following the approach of Love (4) for incompressible materials the product $\lambda \epsilon_{kk}$ is replaced by a finite quantity, $-\Phi$, representing the hydrostatic pressure. Mathematically this substitution implies that as the trace of the strain tensor, ϵ_{kk} , approaches zero the Lamé constant, λ , or equivalently the bulk modulus, K , becomes unbounded in such a manner that the trace of the stress tensor, σ_{kk} , remains finite.

The boundary conditions for this problem are of a mixed type. Small contact pressures exerted by the pericardium as well as small hydrostatic pressures in the thoracic cavity are ignored. The resulting boundary condition is

$$\sigma_{rr}(r_e, t) = 0 \quad . \qquad 2.2.5$$

The displacement boundary condition on the internal surface of the shell is derived as follows.

$$V_i = \frac{4}{3}\pi R_i^3 = V_{io} + \Delta V \sin \omega t \quad ; \quad \omega = 2\pi f \qquad 2.2.6$$

where $V_{io} = \frac{4}{3}\pi r_i^3$ is the instantaneous unperturbed ventricular volume and ΔV and f are the perturbation volume and frequency, respectively. Solution of Equation 2.2.6 for R_i under the assumption of small deformations, $\frac{\Delta V}{V_{io}} << 1$, leads to

$$R_i(t) = r_i\left(1 + \frac{\Delta V}{3V_{io}} \sin \omega t\right) \quad . \qquad 2.2.7$$

The time dependent portion of Equation 2.2.7 is the displacement boundary condition on the inner surface of the shell.

$$u_r(r_i, t) = \frac{r_i \Delta V}{3V_{io}} \sin \omega t \qquad 2.2.8$$

2.3 Solution and Interpretation

The incompressibility condition expressed in spherical coordinates for point symmetric deformations is

$$\epsilon_{kk} = \nabla \cdot \bar{u} = \frac{1}{r^2}\frac{\partial}{\partial r}(r^2 u_r) = 0 \quad . \qquad 2.3.1$$

This expression can be integrated directly and the undetermined function of time evaluated by applying boundary condition 2.2.8.

$$u_r = \frac{g(t)}{r^2} \qquad 2.3.2$$

$$g(t) = \frac{r_i^3 \Delta V}{3 V_{io}} \sin \omega t \qquad 2.3.3$$

The displacement field is then given by

$$u_r(r,t) = \frac{r_i^3 \Delta V}{3 r^2 V_{io}} \sin \omega t \quad . \qquad 2.3.4$$

Combination of Equations 2.2.1 to 2.2.4 leads to the equilibrium equation in terms of displacements.

$$-\Phi_{,i} + \mu u_{i,jj} = \rho_w \ddot{u}_i \qquad 2.3.5$$

$$-\nabla \Phi + \mu \nabla^2 \bar{u} = \rho_w \ddot{\bar{u}} \qquad 2.3.5a$$

By writing Equation 2.3.5a in spherical coordinates and restricting the motion to point symmetric deformations we obtain

$$-\frac{\partial \Phi}{\partial r} = \rho_w \ddot{u}_r \quad . \qquad 2.3.6$$

The Laplacian of the displacement field vanishes because the material is incompressible and the displacements are irrotational. The result of carrying out the integration with the aid of Equation 2.3.4 is

$$\Phi(r,t) = -\frac{\rho_w r_i^3 \Delta V \omega^2}{3 V_{io} r} \sin \omega t + h(t) \quad . \qquad 2.3.7$$

The undetermined function of time is evaluated by direct substitution into the constitutive law for the radial direction with subsequent application of the boundary condition on the exterior surface of the shell.

$$\sigma_{rr}(r,t) = -\Phi + 2\mu \frac{\partial u_r}{\partial r} \qquad 2.3.8$$

$$\sigma_{rr}(r,t) = \frac{\rho_w r_i^3 \Delta V \omega^2}{3 V_{io} r} \sin\omega t - h(t) - \frac{4\mu r_i^3 \Delta V}{3 r^3 V_{io}} \sin\omega t \qquad 2.3.8a$$

$$\sigma_{rr}(r_e,t) = 0 \rightarrow h(t) = \left(\frac{\rho_w r_i^3 \Delta V \omega^2}{3 V_{io} r_e} - \frac{4\mu r_i^3 \Delta V}{3 V_{io} r_e^3} \right) \sin\omega t \qquad 2.3.8b$$

$$\sigma_{rr}(r,t) = \frac{r_i^3 \Delta V \sin\omega t}{3 V_{io}} \left[\rho_w \omega^2 \left(\frac{1}{r} - \frac{1}{r_e}\right) - 4\mu \left(\frac{1}{r^3} - \frac{1}{r_e^3}\right) \right] \qquad 2.3.8c$$

For an incompressible, isotropic material the shear modulus, μ , is related to Young's modulus, E , by the expression, $\mu = \frac{E}{3}$. Imposing this restriction on Equation 2.3.8c and evaluating the stress at the inner surface, $r = r_i$, we find

$$\sigma_{rr}(r_i,t) = -\frac{\Delta V \sin\omega t}{3 V_{io}} \left\{ \frac{4}{3} E \left[1 - \left(\frac{r_i}{r_e}\right)^3 \right] - \rho_w r_i^2 \omega^2 \left(1 - \frac{r_i}{r_e}\right) \right\} . \qquad 2.3.9$$

This stress is the time dependent pressure perturbation, $-\Delta p \sin\omega t$, associated with the volumetric perturbation, $\Delta V \sin\omega t$. The amplitude of this pressure perturbation is

$$\Delta p = \frac{\Delta V}{3 V_{io}} \left\{ \frac{4}{3} E \left[1 - \left(\frac{r_i}{r_e}\right)^3 \right] - \rho_w r_i^2 \omega^2 \left(1 - \frac{r_i}{r_e}\right) \right\} . \qquad 2.3.10$$

As anticipated the internal boundary stress is composed of terms reflecting the elasticity of the wall material and the inertia of the wall itself. Intuitively one would expect that the inertia term would add directly to the stress required to accommodate a prescribed volume perturbation. However, Equation 2.3.10 indicates that inertia acts to relieve the internal boundary stress, and no stress is required for volumetric perturbation if the frequency is sufficiently large. When the circular frequency, ω, takes on the value

$$\omega = \left\{ \frac{4E\left[1-\left(\frac{r_i}{r_e}\right)^3\right]}{3\rho_w r_i^2\left(1-\frac{r_i}{r_e}\right)} \right\}^{1/2} \qquad 2.3.11$$

the pressure at the inner wall is zero which corresponds to the case of free point symmetric vibrations.

Equation 2.3.10 can be rearranged into a form that suggests how the effective Young's modulus can be inferred from a properly designed experiment.

$$E = \frac{9}{4}\,\frac{V_{io}}{1-\left(\frac{r_i}{r_e}\right)^3}\,\frac{\Delta p}{\Delta V} + \frac{3}{4}\rho_w r_i^2 \omega^2 \frac{1-\frac{r_i}{r_e}}{1-\left(\frac{r_i}{r_e}\right)^3} \qquad 2.3.12$$

or

$$E = \frac{9}{4}\,\frac{V_{io}(V_{io}+V_w)}{V_w}\,\frac{\Delta p}{\Delta V} + \frac{3}{4}\rho_w \omega^2 \left(\frac{3V_{io}}{4\pi}\right)^{2/3}\left[1-\left(\frac{V_{io}}{V_{io}+V_w}\right)^{1/3}\right]\left(\frac{V_{io}+V_w}{V_w}\right) \qquad 2.3.13$$

where $\frac{\Delta V}{\Delta p}$ = overall distensibility, and V_w is the wall volume. The first term represents a perturbation of Lamé's classic solution for a thick-walled spherical shell, and the second term incorporates the effects of wall inertia. The static term is presented in parametric form in Figure 3.

The next chapter deals with the experimental determination of distensibility, and in Chapter 5 the appropriate geometric parameters are applied to Equation 2.3.12 to compute the effective Young's modulus of the ventricular wall.

3. DETERMINATION OF VENTRICULAR DISTENSIBILITY BY GENERATING ARTIFICIAL HEART SOUNDS

The distensibility of the left ventricle is a dynamic variable since there are sizeable changes in geometry and presumably substantial changes in the elastic properties of the ventricular wall that occur during the cardiac cycle. Therefore, the techniques employed to determine distensibility should preserve the in vivo environment and should yield essentially instantaneous values. These techniques are based on obtaining the pressure response of the ventricular cavity to an imposed volumetric perturbation. For a given ventricular configuration and assuming linear elastic behavior of the myocardium, the pressure response to volumetric perturbations can be interpreted as a measure of the "effective Young's modulus" of the ventricular wall. In the distensibility studies performed on the apex of the left ventricle by Adolph (5), the time dependence of the ventricular configuration and of the wall properties was suppressed by reducing the heart rate with drugs.

Initially a spring-loaded syringe was used for injecting various amounts of saline solution into the left ventricles of anesthetized dogs with open chests. The induced pressure change was measured with the aid of a catheter-tipped manometer located in the ventricle. These injections could be timed to coincide with any phase of the cardiac cycle. Examples of data taken with this technique are shown in Figures 4 and 5. Several disadvantages are apparent:

1. The repeatability of the pressure response for a given volumetric change at a given point in the cardiac cycle was unsatisfactory.

2. It was difficult to assess the exact shape of the pressure curve if no injection had occurred.

3. Volume and pressure perturbations were not consistent with the small deformation analysis of Chapter 2.

Aiming for a higher degree of accuracy and a better defined perturbation, an electrically driven piston, whose volumetric displacement and frequency could be accurately controlled, was inserted into the left ventricle. The resulting pressure signals produced by this vibrating piston are termed "artificially induced heart sounds" because the experimental frequency range, 20 to 200 Hz, coincides with the audible band that contains most of the phonocardiographic information. The next sections describe the application of this technique.

3.1 Surgical Preparation and Instrumentation

Mongrel dogs of uncertain age weighing between 23 and 34 kg were anesthetized by an intravenous injection of 30 mg of Nembutal per kilogram of body weight. Additional anesthesia was administered as needed. With the dog in the supine position, a cannula mounted on a P23Dd Statham arterial pressure transducer was inserted into the left femoral artery and advanced to the bifurcation. Following surgical exposure of the left common carotid artery, a catheter-tipped Bytrex manometer was inserted into that vessel and advanced down the arterial tree into the left ventricle. The animal was ventilated through an endotracheal catheter by a Palmer respirator at approximately 10 liters/minute. The thorax was opened longitudinally along the length of the sternum as well as transversely along the fifth left intercostal space. To minimize local bleeding the internal thoracic artery and vein were tied off.

A rubber finger from a surgical glove was stretched over the sleeve of the Goodmans VP4 vibrator shown in Figure 6. The volumetric displacement characteristics, Figure 7, had previously been determined by optically tracking* the piston travel for various frequencies at back pressures up to 150 mm Hg. No apparent back pressure effects were observed.

---

*PhysiTech, Inc.
Model 39A Electro-optical Tracking Unit

The pericardium which surrounds the heart was cut directly above the left atrium. A small exposure was mandatory so as to minimize the effects of any reduction of the support function of that membrane. The left atrial appendage was surgically opened and the vibrator advanced through the mitral valve into the ventricle. The atrium was then tied with umbilical tape. The piston apparently did not substantially obstruct the pulmonary venous return or the mitral valve function since the heart rate and ventricular pressure returned to normal levels within a few minutes after insertion. With the aid of an X-ray fluoroscope the vibrator tip was positioned above the papillary muscles. The pressure transducer was located lateral to the axis of the vibrator sleeve and slightly behind its tip so as to minimize any dynamic pressure effects caused by the piston motion. Finite trains of sinusoidal piston motion were generated by a Hewlett-Packard (model 204B) oscillator, a General Radio Company (model 1396-A) tone burst generator and a high fidelity amplifier in series with the vibrator. Arterial and intraventricular pressures were recorded on a Honeywell 1108 Visicorder equipped with M3300 fluid damped galvanometers.

At the conclusion of the experiment the intracardiac transducer was calibrated with the aid of the Statham arterial monitor. The recording system had a resolution limit of 1 mm Hg for the amplifier gain settings used during these experiments.

3.2 Data Acquisition and Reduction

The entire perturbation frequency range, 20 to 200 Hz, was covered within five minutes, and during that time there appeared to be no adverse effect on systolic pressure due to the imposed vibrations. Figures 8 and 9 show typical intraventricular pressure response profiles which resulted from the imposed volumetric perturbations. Distensibility was calculated as the ratio of volumetric displacement, ΔV , and the measured peak-to-peak pressure change, Δp . Below 25 Hz the height of the pressure perturbation could not be accurately determined because the period of the sinusoidal vibration was approaching the order of the systolic ejection time. The absence of pressure variations during the diastolic filling phase is particularly significant, and its interpretation will be given in Chapter 5. The minimum ventricular pressure or filling pressure was obtained with the aid of the Bytrex transducer.

3.3 Results

The dependence of ventricular distensibility on the perturbation frequency during systolic ejection is shown in Figures 10 to 13. Each point represents an average of the data obtained from five to ten cardiac cycles. The distensibility was found to vary from dog to dog due, perhaps, to uncertainties in age, breed and medical history. However, in all cases the distensibility increases from approximately 25 Hz to a maximum in the vicinity of 60 to 90 Hz and then diminishes with increasing frequency. Within an individual experiment the distensibility at systole did not vary noticeably during the ejection phase.

The unexpected peaking of the distensibility curve has yet to be explained. It could conceivably be a manifestation of a viscoelastic wall or an artifact. The qualitative explanation for this artifact could be a variation in the skirting of the rubber finger with frequency. As illustrated in Figure 14 it is possible that at low frequencies where the inertia of the rubber is negligible the actual volumetric displacement induced by the piston was greater than that calculated from the piston travel. Therefore the experimental distensibility data represent a lower bound for the actual distensibility of the ventricular cavity.

4. FREQUENCY SPECTRA OF THE FIRST AND SECOND NATURALLY OCCURRING HEART SOUNDS

Both standard chest phonocardiography and stethoscopic auscultation techniques are subject to limitations which obscure information on the mechanical behavior of the heart. In each case sound vibrations that reach the chest have been transmitted through intermediate anatomical structures which attenuate and distort the spectral distribution (6). The stethoscope further modifies the sound by introducing amplification due to resonance of the instrument.

Intracardiac phonocardiography, pioneered by Soulié, Yamakawa, Lewis and Luisada and Liu, represented a significant step toward eliminating the unknown effects of intermediate structures (7). Spectral analysis of chest recorded heart sounds using digital computers was investigated by Gerbarg et al (8). The purpose of the present study is to obtain frequency spectra for the first and second heart sounds by combining intracardiac phonocardiography and electronic filtering. This spectral analysis is performed within the audible frequency band, 20 to 200 Hz.

When heart sounds are generated both the ventricular wall and the enclosed fluid mass are set into transient vibration. These vibrations are manifested as sound pressure fluctuations which are superimposed on the gross pressure variations of the cardiac cycle. These sound perturbations are not seen on pressure recordings obtained by intracardiac transducers with fluid filled cannuli because the frequency band of the sounds exceeds the fundamental frequency of the transducer-cannula system.

The separation of these sound vibrations from the gross pressure fluctuations requires a highly sensitive transducer, selective filtering and a high degree of amplification. An extremely sensitive transducer, originally designed for wind tunnel applications by the Schaevitz-Bytrex Company (model HFD-5), has been adapted for physiologic use by mounting it at the end of a catheter. This transducer has a flat response from dc to 60 kHz and has a maximum resolution of 0.1 mm Hg when energized by a 25v dc source at maximum amplifier gain. Amplification levels sufficient for signal visualization were accomplished by Astrodata 885 wideband differential dc amplifiers with a variable gain up to 3000. A Krohn-Hite (model 330M) ultra-low frequency variable band-pass filter, set for minimum band-width, was used for sound decomposition. The roll-off characteristic of this filter is shown in Figure 15. It also has the high damping characteristics required for the analysis of transient heart sounds.

Unfortunately any filter with a good transient response characteristic inherently possesses a relatively low attenuation slope which for this filter is 18 db/octave. The Krohn-Hite (model 330M) is a fixed percentage band-width filter whose attenuation skirt terminates at approximately $0.2f_c$ and $4.2f_c$ where f_c is the variable center frequency. Only those frequency components of the input signal that are contained within these limits will be passed through the filter. The degree to which each component is present in the output is determined by the attenuation characteristic of the filter and the energy distribution of the input. Figure 16 illustrates schematically the effect of this broad skirt width for a filter operating within the hypothetical Fourier spectrum of the intraventricular pressure profile. When the lower limit of the skirt lies near the fundamental frequency of the heart, f_n, the dominant component of the output is usually not the center frequency of the filter. The amplitude of the low frequency Fourier components is so great that, even after attenuation, their presence can be seen in the filter output in the form of a reduction in the frequency of the filtered signal relative to the center frequency.

This effect diminishes rapidly with increasing center frequency for intraventricular spectra and is less pronounced over the entire frequency range when spectral analysis is performed in the ascending aorta where the gross pressure fluctuations are considerably less than in the ventricle. Despite this disadvantage new information on heart sound spectra in the audible frequency range has been obtained.

4.1 Surgical Preparation

As in the distensibility experiments Nembutal anesthesia was used, and the animal was placed in the supine position. Normal respiration was maintained throughout the experiments and was monitored by the electrical output of a mercury-filled silastic tube sutured to the chest. A standard lead II electrocardiogram recorded the electrical activity of the heart and served as an aid in ascertaining the validity of the filtered sounds. Again a P23Dd arterial Statham transducer with a radio-opaque cannula was inserted into the left femoral artery and the tip positioned at the femoral bifurcation. The left heart was catheterized with a Bytrex transducer via the left common carotid artery. Extreme care was taken not to damage the aortic valve leaflets. With the aid of an X-ray fluoroscope the transducer tip was positioned approximately midway between the papillary muscles and the aortic valve. Positions below the papillaries resulted in artifacts due to contact pressure between the transducer and the endocardial surface.

4.2 Data Acquisition and Reduction

In analyzing the heart sounds the amplifier gain setting was kept constant for the entire frequency range. By adjusting this gain for maximum galvanometer deflection at 20 Hz, consistent with recording paper width, an acceptable level of resolution could be obtained at the selected upper frequency limit of 200 Hz. Data recordings were first taken with the pressure sensor located within the left ventricle for filter settings ranging from 20 to 200 Hz. The transducer was then retracted from the ventricle and positioned in the ascending aorta approximately one to three centimeters above the aortic valve, and the filtering procedure was repeated without altering the amplifier gain settings. Typical sound tracings from the ventricle and ascending aorta are shown in Figures 17 and 18, respectively.

The experiments were concluded with an in vivo calibration of the heart sound transducer. To this end a second Bytrex transducer, of known sensitivity, was inserted into the right common carotid artery and positioned with the heart sound transducer in the same cross-section of the descending aorta. The aorta was exposed by an incision through the seventh left intercostal space. A wave generator (see Figure 6) was positioned over the aorta approximately six centimeters below the transducers as shown in Figure 19. Gated trains of sinusoidal pressure waves were propagated in the retrograde direction by tapping the aortic wall at discrete frequencies ranging from 20 to 200 Hz. By adhering to this procedure it was possible to determine the sensitivity of the heart sound transducer, including the filtering and recording system, as a function of frequency.

Data reduction consisted of measuring the peak-to-peak galvanometer deflections, A_1 and A_2 , of the first and second sounds, respectively, over one respiratory cycle for each filter frequency. These deflections were converted into sound pressure by making use of the calibration described above.

4.3 Results

Figures 20 to 22 represent uncorrected sound spectra for the left ventricle and the ascending aorta averaged over one respiratory cycle. These spectra are uncorrected in the sense that they contain, in varying degrees, the attenuated low frequency Fourier components of the pressure pulse that were described in section 4. The presence of these attenuated components was particularly noticeable below 50 Hz on the filtered traces from the ventricle. Below 50 Hz the period, T, of the filtered sound was larger than that corresponding to the band-pass center frequency. This effect was less pronounced above 50 Hz for the intraventricular spectra and above 30 Hz in the case of the aortic spectra.

In all experiments the intensity of the filtered sounds was greatest at the end of inspiration. When the intrathoracic pressure assumes its minimum value at the end of inspiration the ventricle accommodates a larger fluid volume than at expiration. Consequently, the initial length of the fibers in the myocardium is maximal and results in a more forceful contraction of the ventricle. Associated with this increased force of contraction are larger amplitude vibrations of the fluid-solid system which comprise the heart sounds.

An extensive effort was made to extract the true spectral density from the uncorrected spectra by applying the method of collocation to the following integral.

$$P(f_c) = \int_{f_n}^{\infty} p(f)\ F(f, f_c)\ df$$

where f_c = band-pass center frequency, Hz

f_n = heart rate, Hz

$P(f_c)$ = known filtered distribution

$p(f)$ = true spectral density

$F(f, f_c)$ = filter characteristic

This integral was inverted successfully, but the resulting density distribution did not exhibit a consistent degree of stability and was, therefore, not meaningful.

Physical interpretation of these uncorrected spectra is given in Chapter 5.

5. CONCLUSIONS AND DISCUSSION

The theory proposed in Chapter 2 provides the means of linking the distensibility of the ventricular cavity to the material properties of the myocardium. This conversion is shown in Figures 23 to 26. Both the Lamé solution and wall inertia effects are presented. The internal and external radii, r_i and r_e, were obtained from average ventricular volume and wall thickness measurements at autopsy. The purpose of this conversion was not to obtain exact numerical results from an oversimplified model of the ventricle but rather to demonstrate the order of magnitude of the effective Young's modulus and its frequency dependence. In all cases wall inertia was shown to be negligible below 100 Hz and produced, at most, a 10 per cent increase in the effective modulus at 200 Hz.

During the low pressure filling phase no sinusoidal pressure fluctuations could be observed on the ventricular pressure trace. This observation means that during diastole Δp must have been less than 1 mm Hg, the system resolution limit. For this resolution limit of 1 mm Hg and the same geometrical values used in deriving the systolic modulus, the corresponding effective modulus at 100 Hz is less than 2×10^6 dynes/cm^2. This result indicates that the systolic modulus is about an order of magnitude larger than the diastolic modulus. The results presented here are comparable in magnitude with the dynamic elastic moduli predicted by Lundin (9) using length-tension considerations on an axially vibrating frog heart muscle fiber at 10 Hz. In those experiments the dynamic modulus ranged from 0.08×10^7 to 1×10^7 dynes/cm^2 representing the diastolic and systolic values.

The variation in ventricular wall properties within the cardiac cycle must have an influence on the quality of the sounds produced by the heart. When the first heart sound occurs the ventricle contains its maximum fluid mass, and the myocardium is quite distensible. On the basis of mechanical considerations we intuitively expect that the first sound spectrum should be dominated by low frequency components. Similarly, the second and loudest sound occurs when the enclosed fluid mass is a minimum, and it has been shown that the ventricular wall at this point has a considerably higher degree of rigidity than at diastole. Accordingly we would predict that the spectrum of the second sound should contain more high frequency components than that of the first sound. These predictions are indeed verified by the experimental data given in Figures 21 and 22 which show that the second sound peaks at 45 Hz while the first sound peaks at 30 Hz. The attenuation of the sounds over a 3 cm distance above the aortic valve is nearly independent of frequency as contrasted with the findings obtained for artificial waves in the descending aorta where attenuation is closely related to wavelength and frequency. This suggests that the ascending aorta participates in the generation of heart sounds.

In conclusion, it has been established by direct measurements of the distensibility that the material properties of the left ventricular wall vary with the phase of the cardiac cycle and are frequency dependent within the ejection phase of systole. These results confirm the behavior of intravascularly recorded heart sound spectra.

An increase in the level of theoretical sophistication should be applied only to a more realistic geometric model of the ventricle since it is expected that geometric considerations dominate the combined effects of fluid inertia and compressibility and viscosity.

REFERENCES

1. Rushmer, R.F., Cardiovascular Dynamics, second edition, W.B. Saunders Company, 1964.

2. Guyton, A.C., Textbook of Medical Physiology, third edition, W.B. Saunders Company, 1966.

3. McKusick, V.A., Cardiovascular Sounds in Health and Disease, The Williams and Wilkins Company, 1958.

4. Love, A.E.H., A Treatise on the Mathematical Theory of Elasticity, fourth edition, Dover Publications, 1944.

5. Adolph, Robert J., "Compliance of the Apex of the Left Ventricle in Unanesthetized Dogs," Journal of Applied Physiology 20(4):758-762, 1965.

6. Nickerson, J.L. et al., "Conference on Cardiovascular Sound," American Journal of Cardiology, Vol. 19, April 1967.

7. Laurens, Paul, "Catheterization by an Intracardiac Micromanometer," Intravascular Catheterization, second edition, Charles C. Thomas Publisher, Springfield, Illinois, 1966.

8. Gerbarg, D.S. et al., "Computer Analysis of Phonocardiograms," Medical Electronics in Cardiovascular Disease, Grune and Stratton, 1963.

9. Lundin, Gunnar, "Mechanical Properties of Cardiac Muscle," Acta Physiologica Scandinavica, Vol. 7, Supplementum XX, 1944.

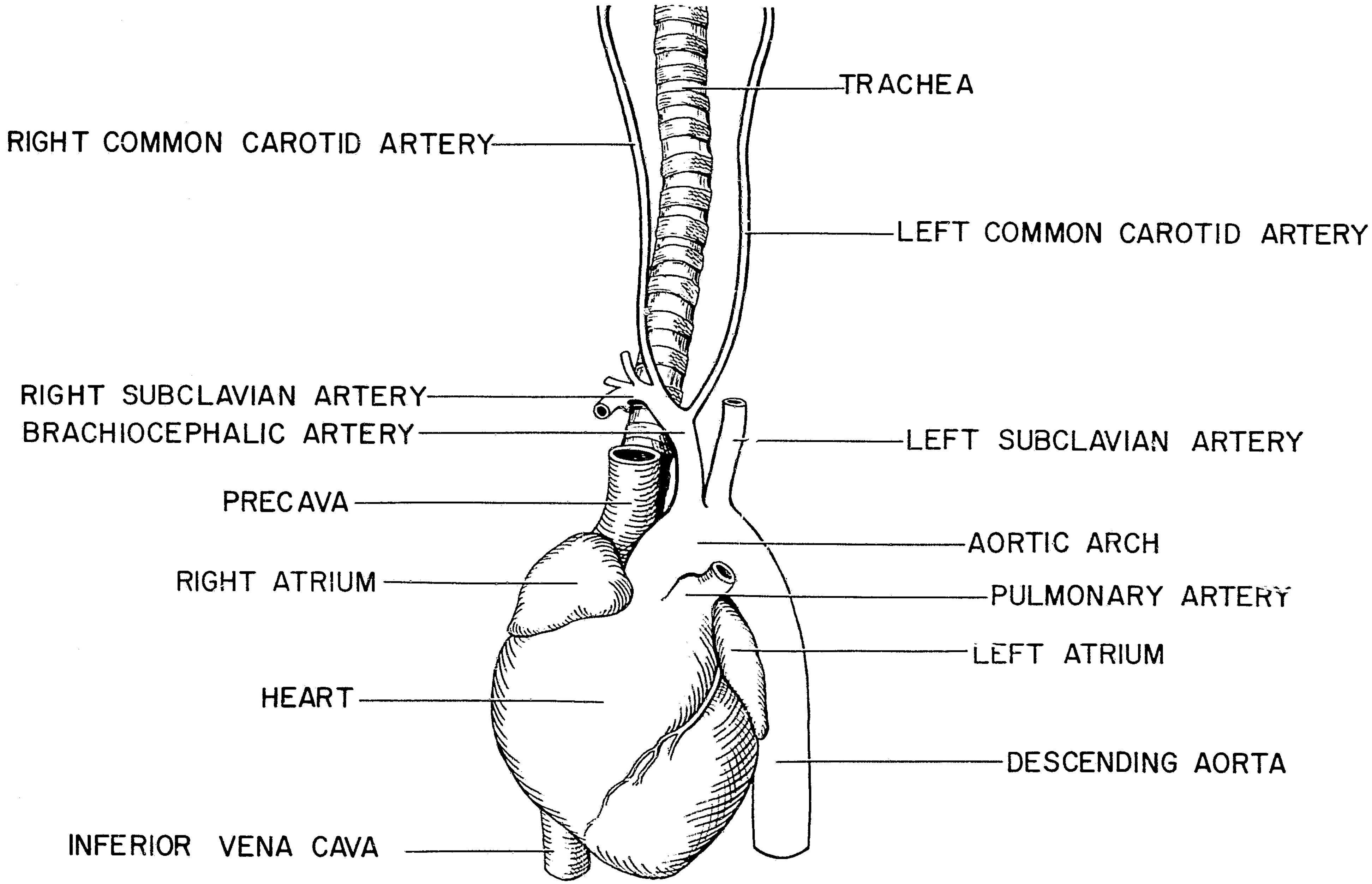

Figure 1. Anatomical Relationship of the Heart and Large Arteries and Veins for the Dog

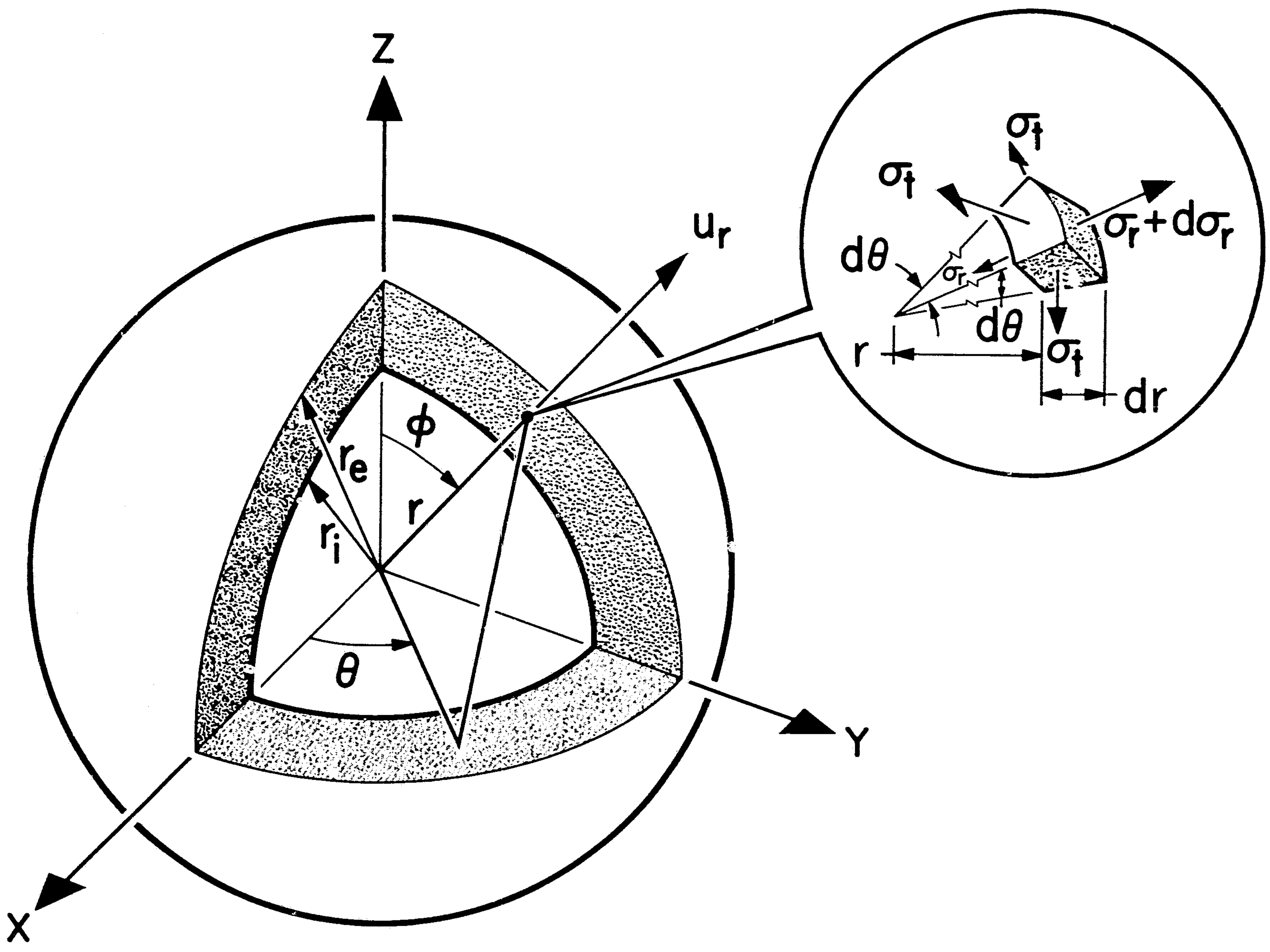

Figure 2. Thick-Walled Spherical Shell Coordinate System

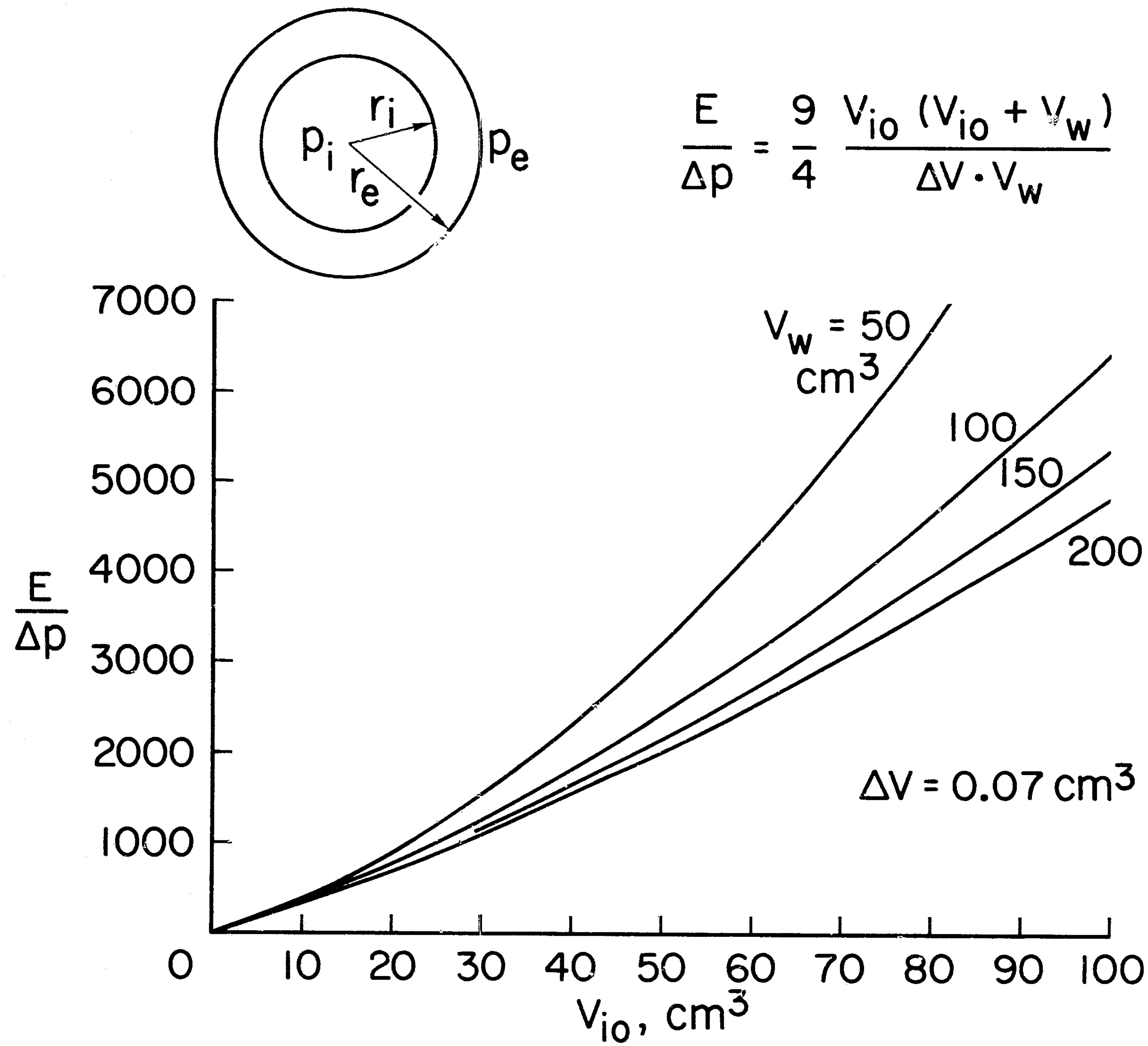

Figure 3. Distensibility of Incompressible Thick-Walled Spherical Shells

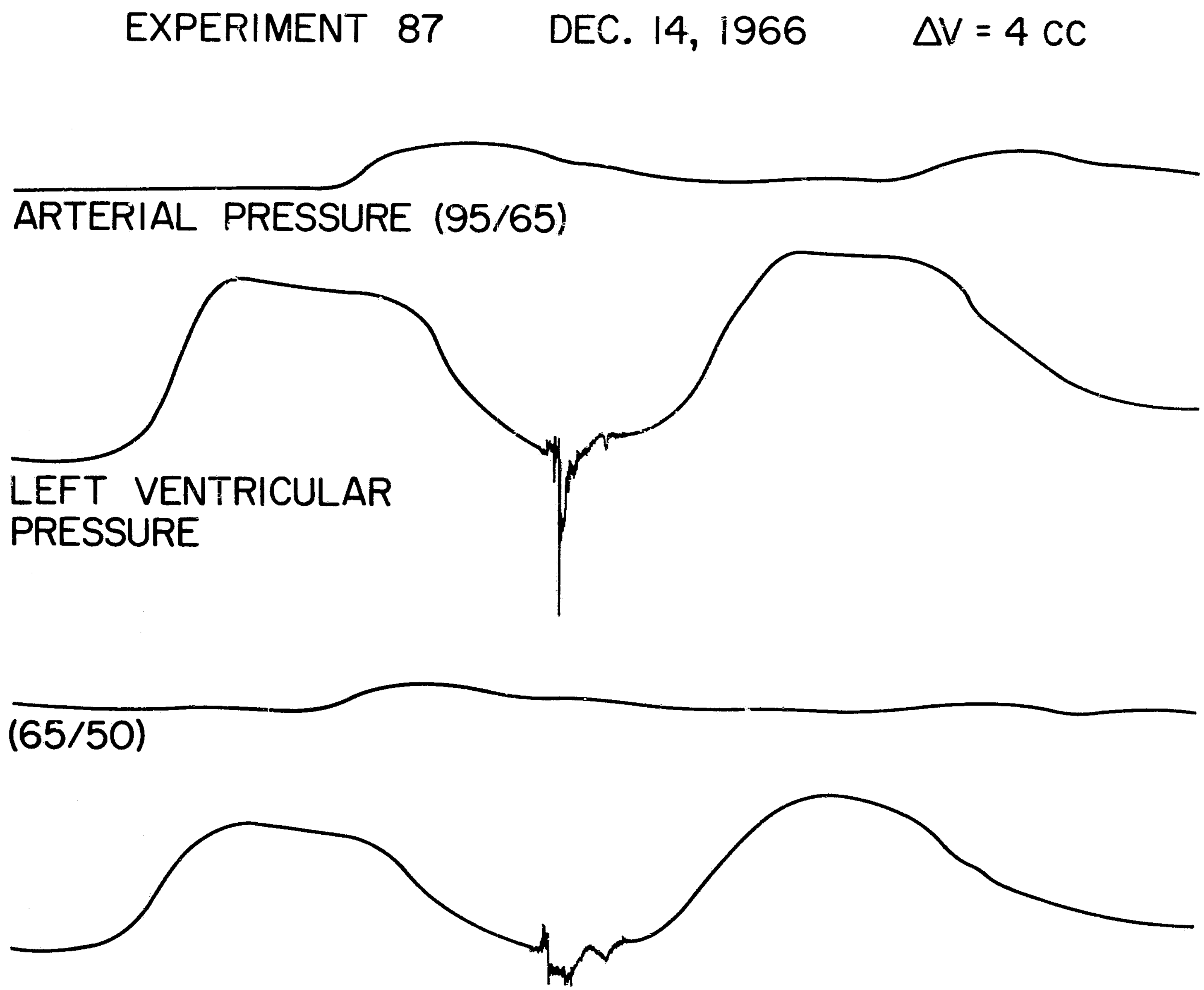

Figure 4. Response of the Left Ventricular Cavity to Rapid Injections of Saline at Diastole

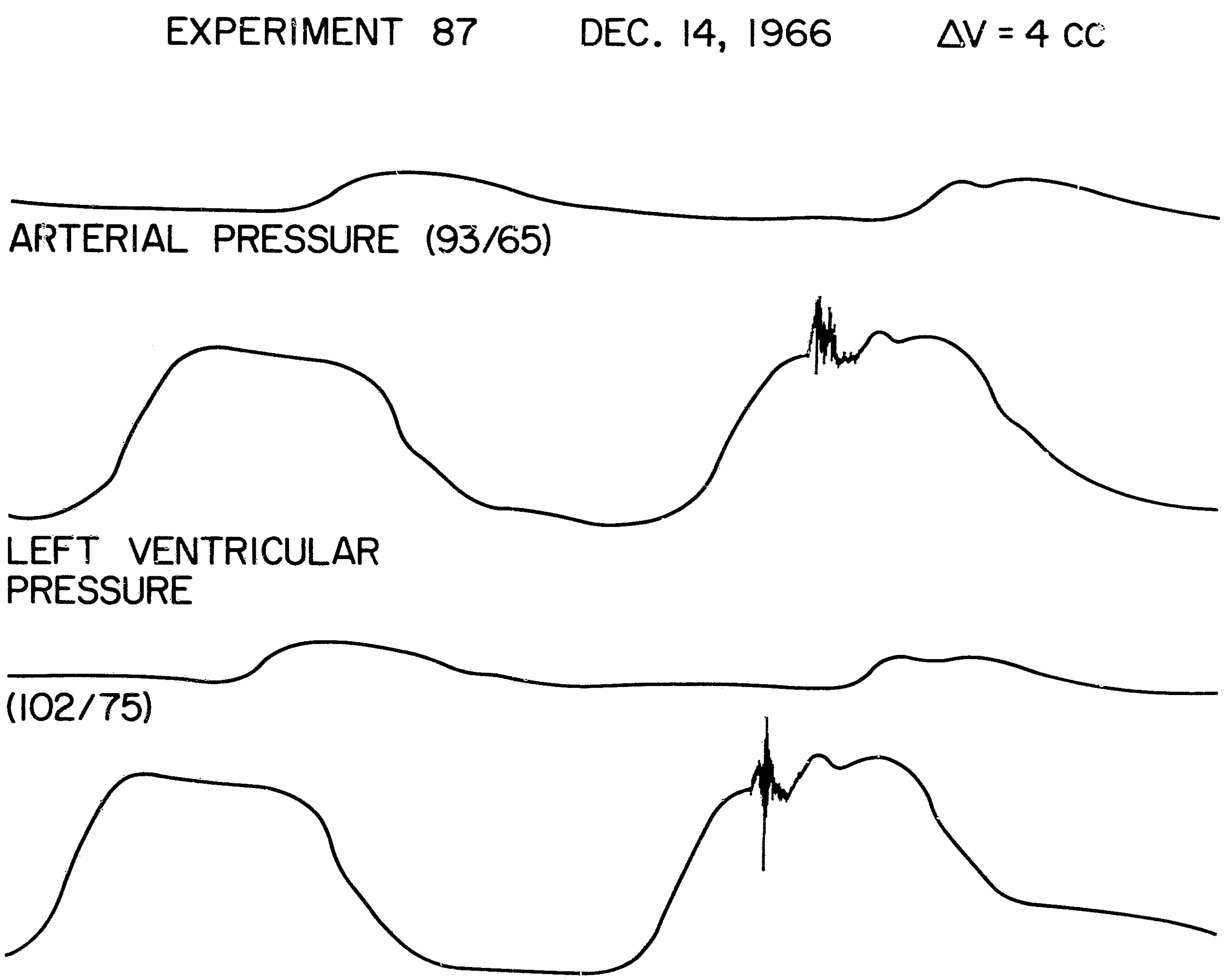

Figure 5. Response of the Left Ventricular Cavity to Rapid Injections of Saline at Systole

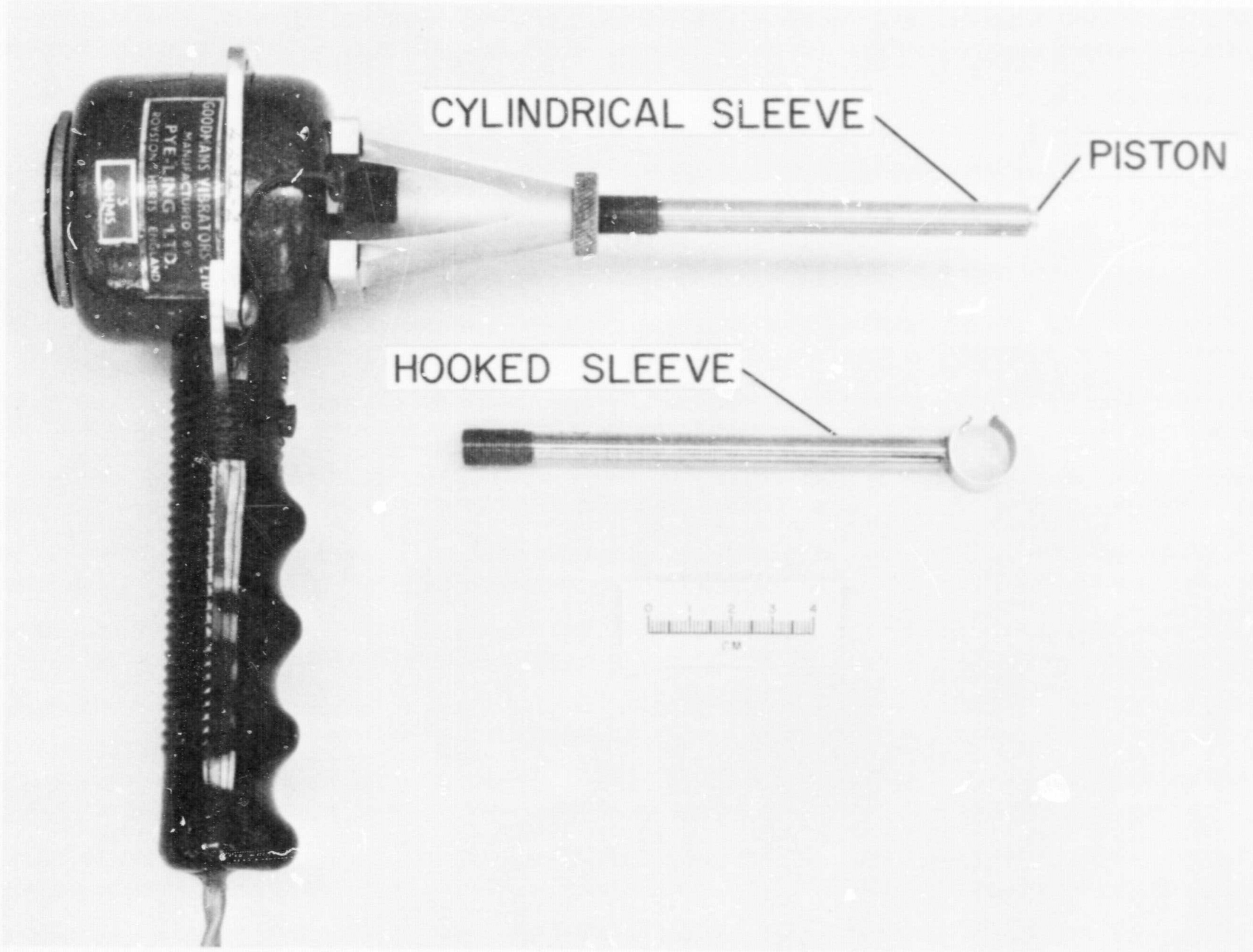

Figure 6. Goodmans Electromagnetic Wave Generator With Interchangeable Sleeves

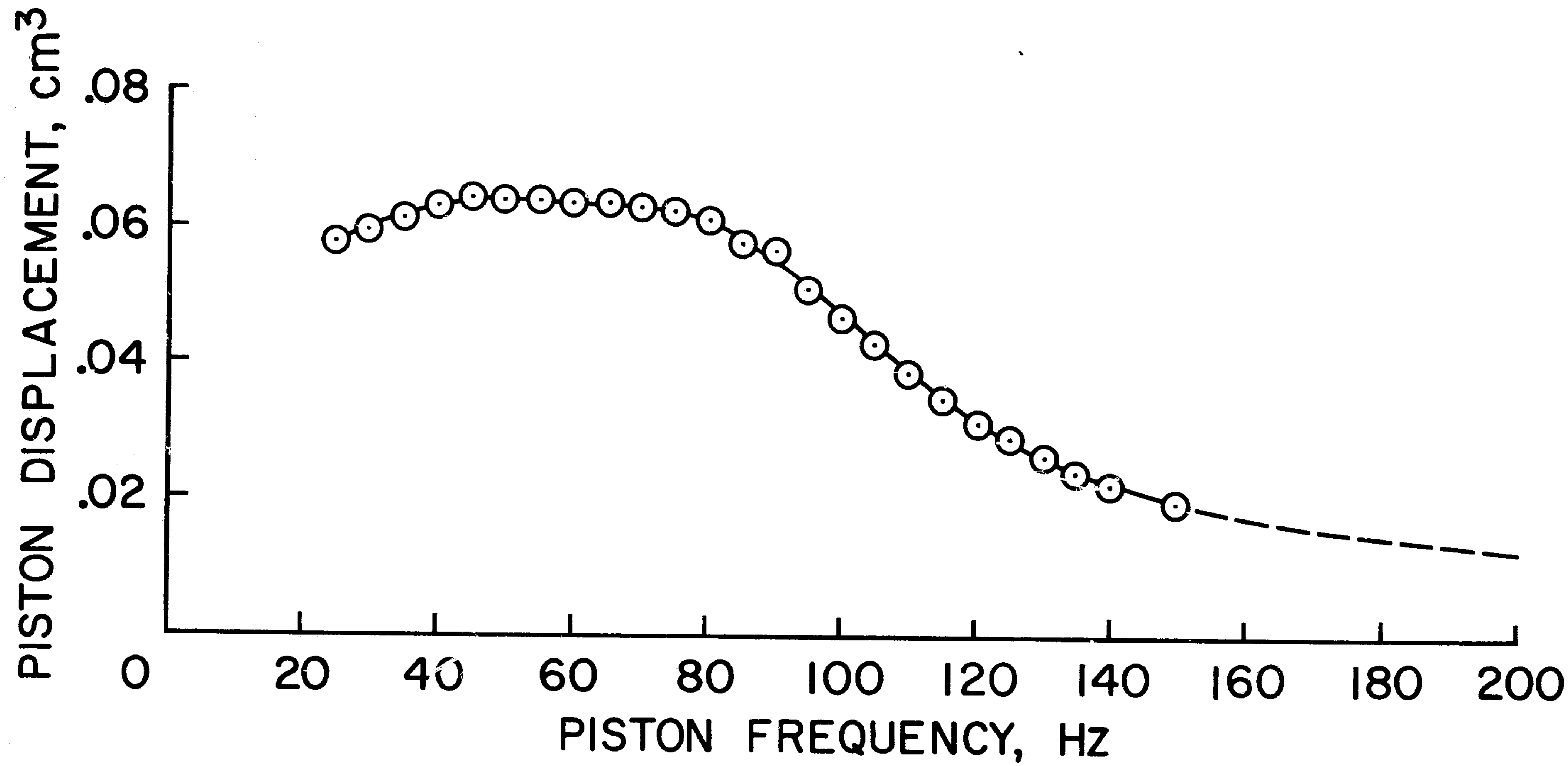

Figure 7. Calibration of Goodmans Vibrator and Piston Assembly

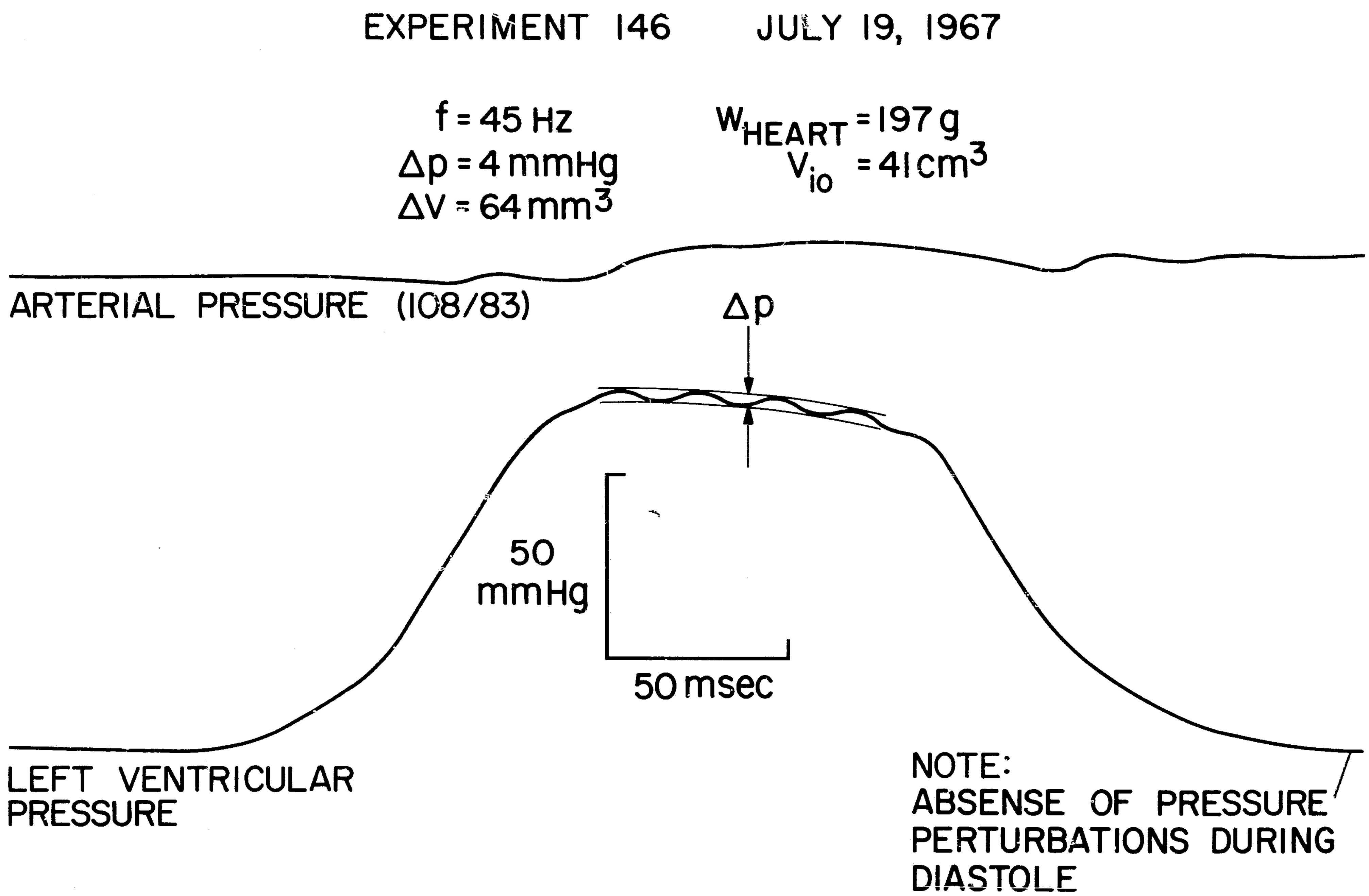

Figure 8. Response of the Left Ventricular Cavity to Artificially Induced Heart Sounds, 45 Hz

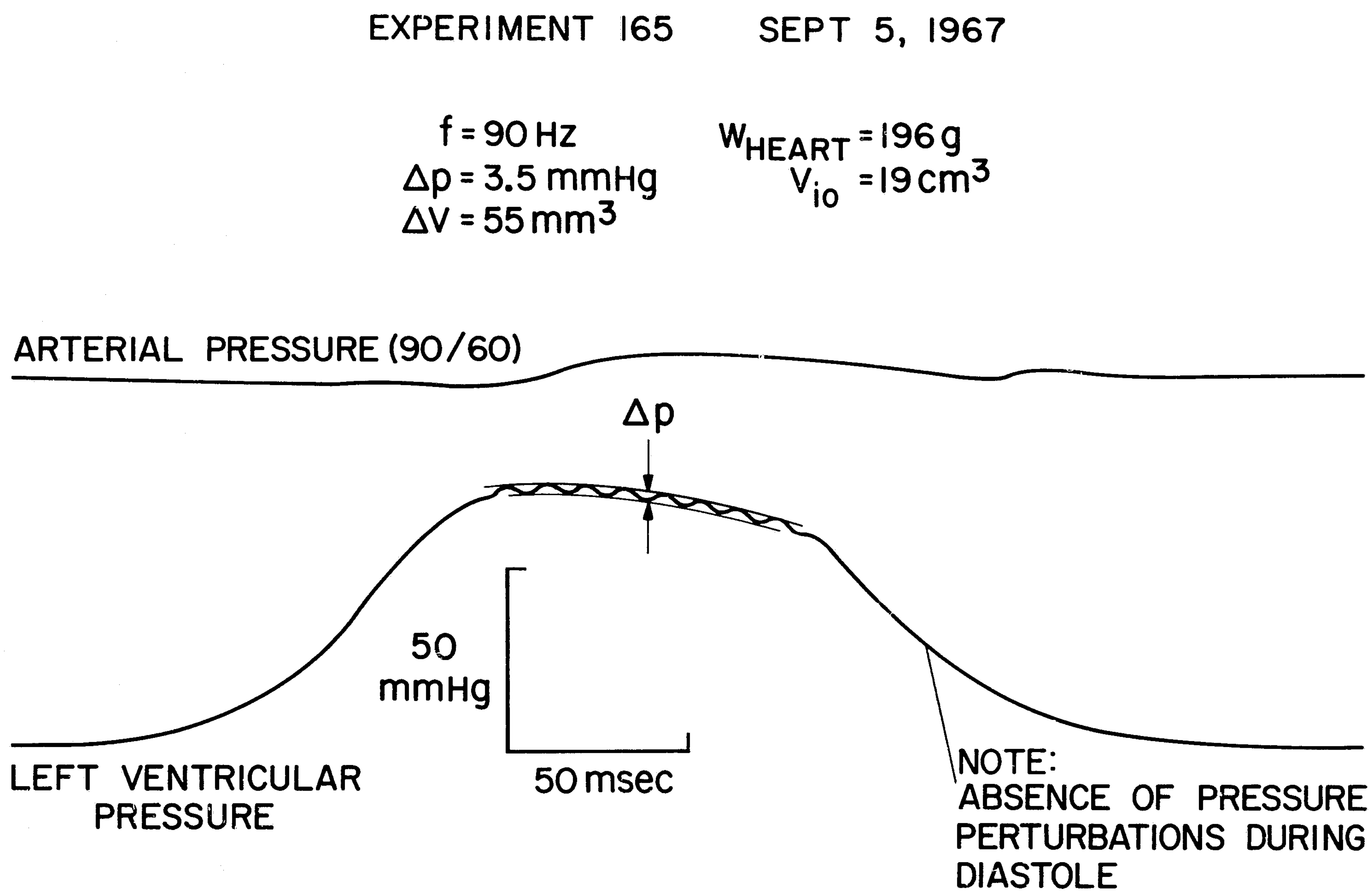

Figure 9. Response of the Left Ventricular Cavity to Artificially Induced Heart Sounds, 90 Hz

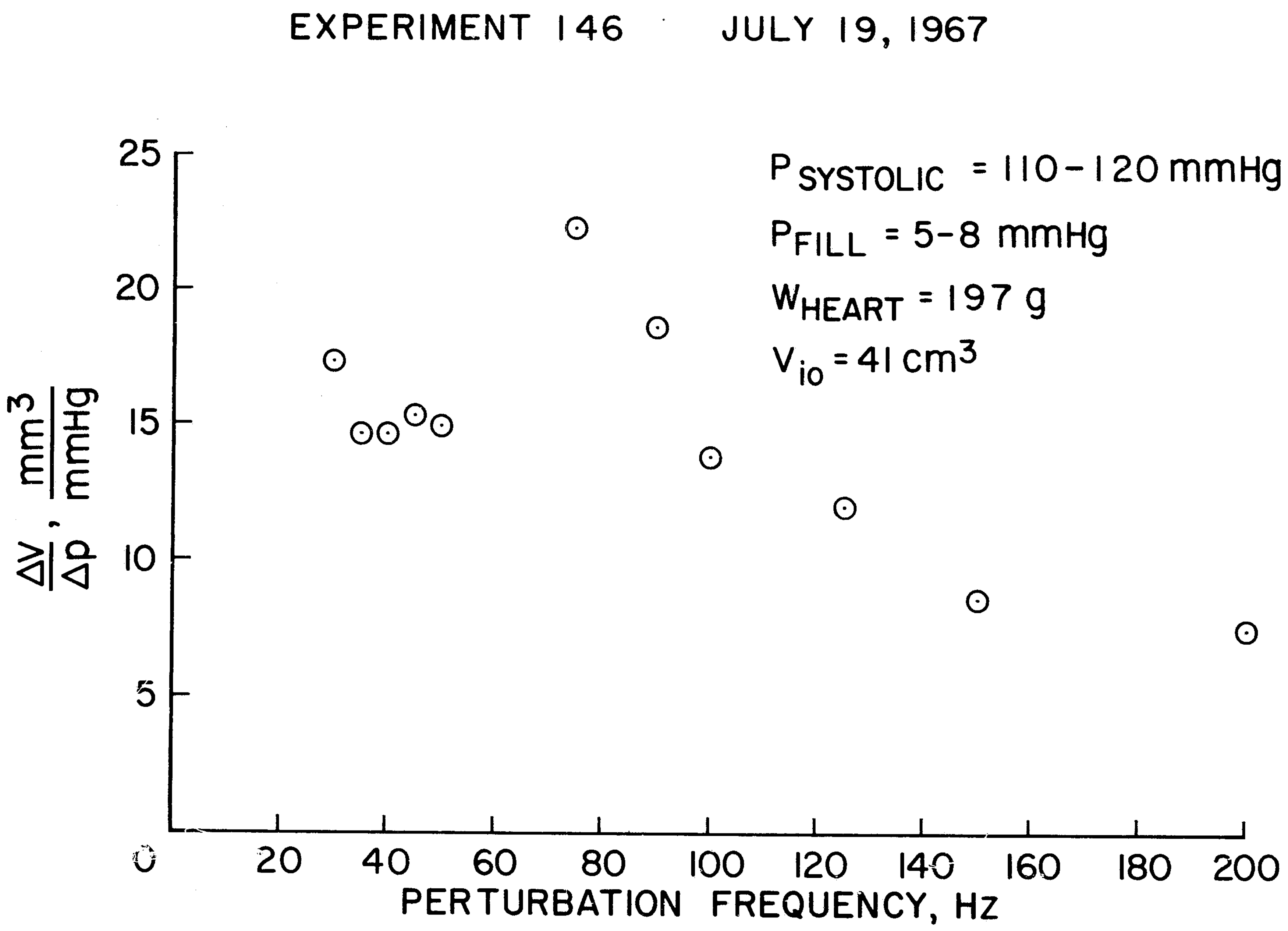

Figure 10. Left Ventricular Distensibility at Systole, Experiment 146

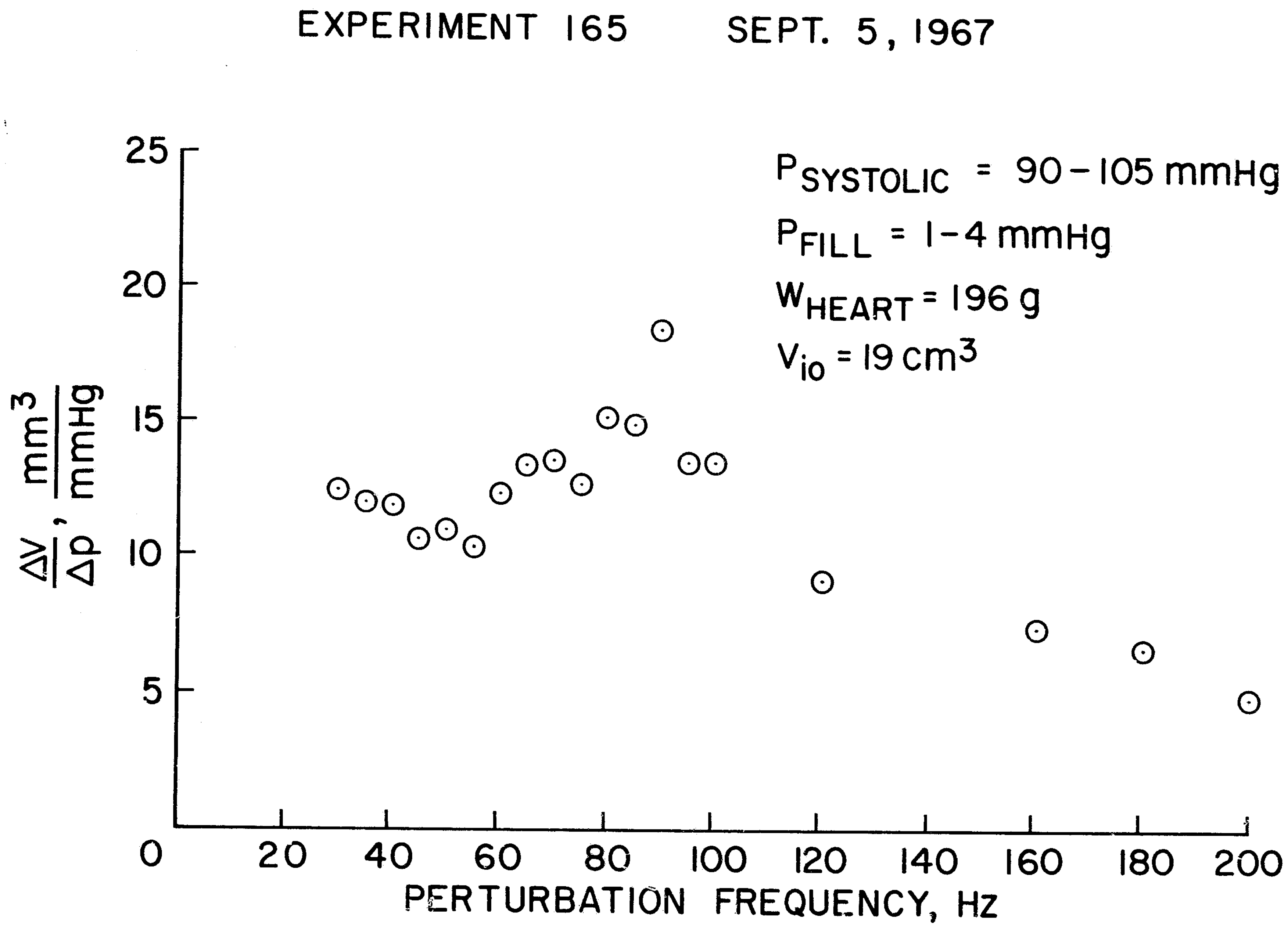

Figure 11. Left Ventricular Distensibility at Systole, Experiment 165

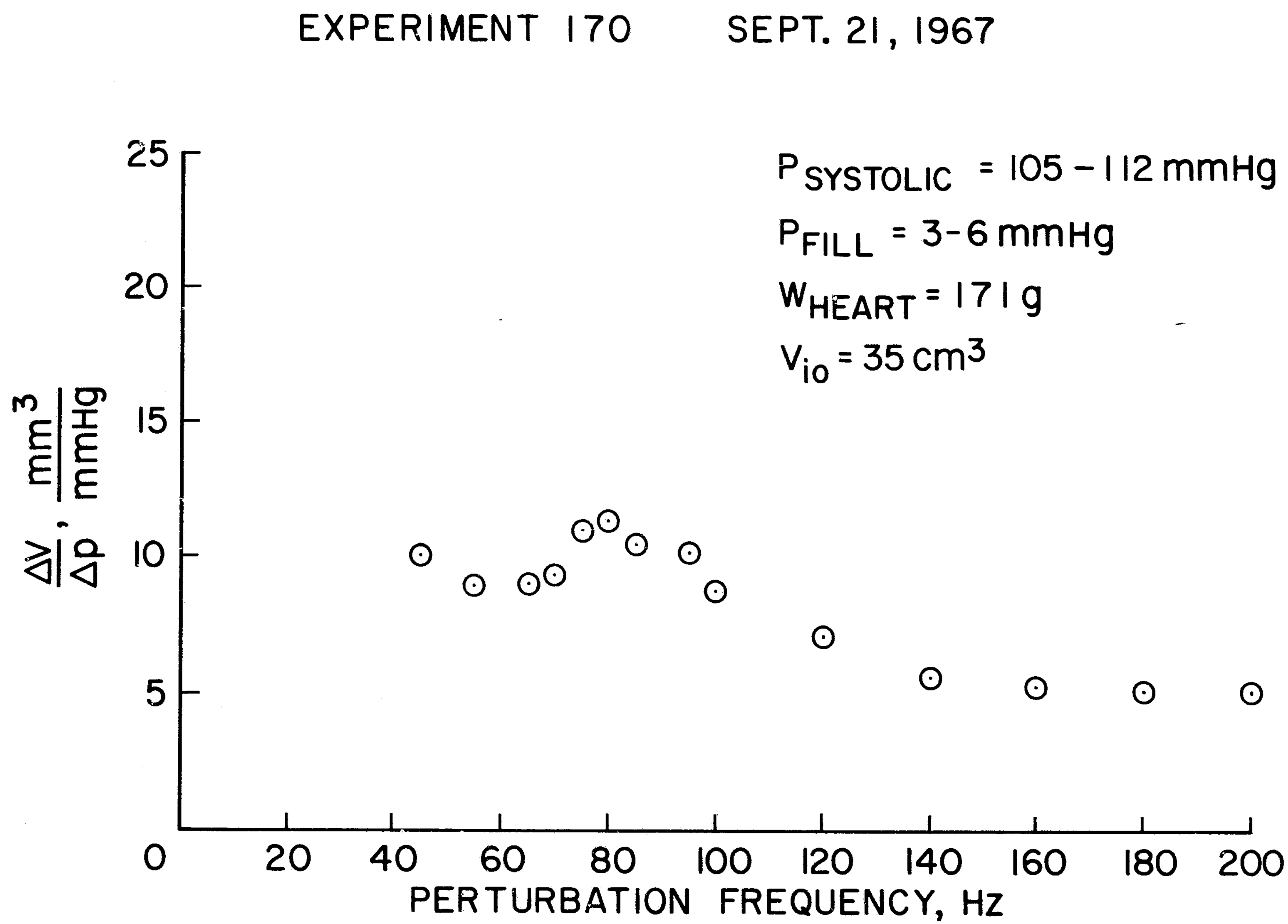

Figure 12. Left Ventricular Distensibility at Systole, Experiment 170

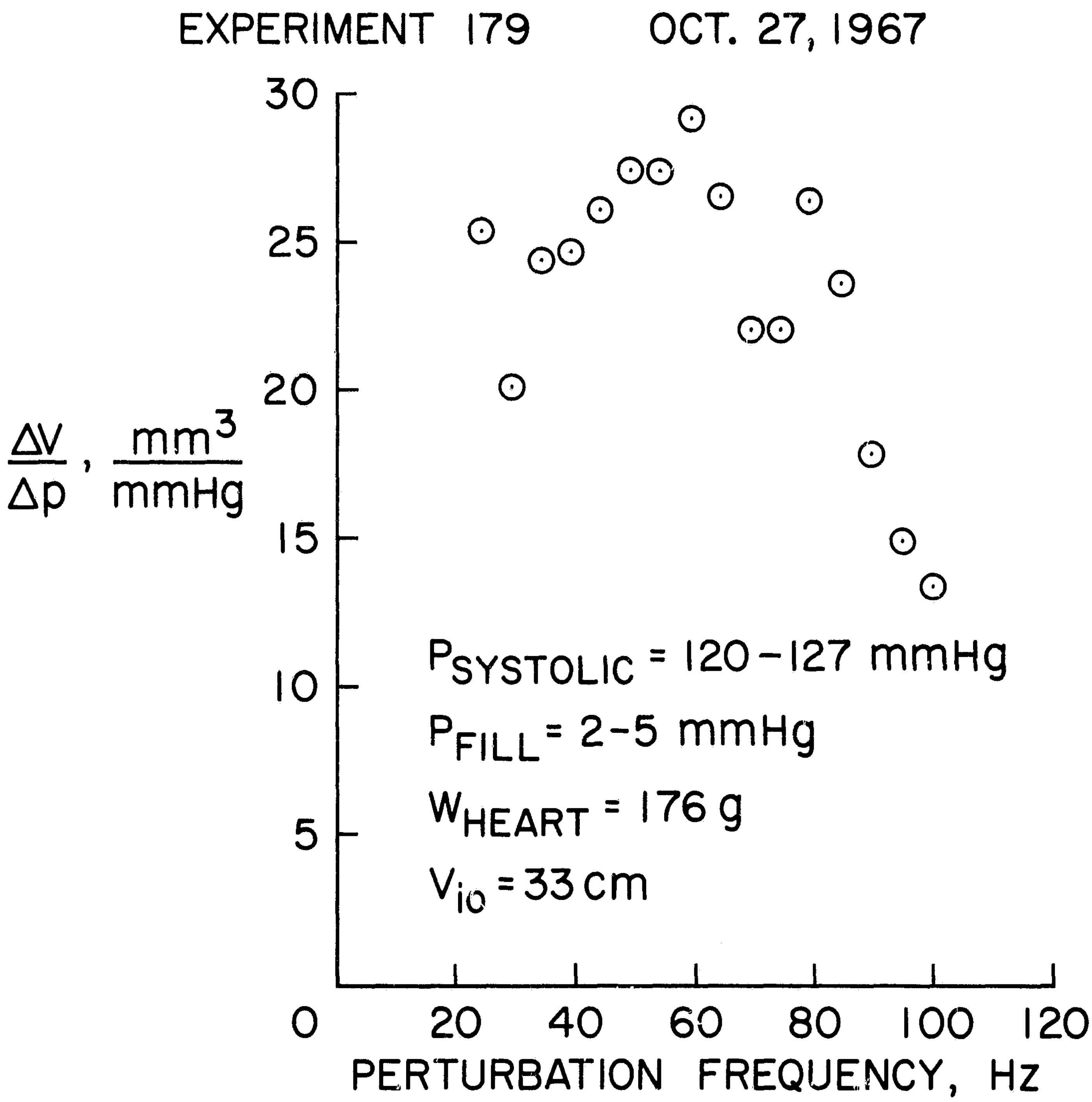

Figure 13. Left Ventricular Distensibility at Systole, Experiment 179

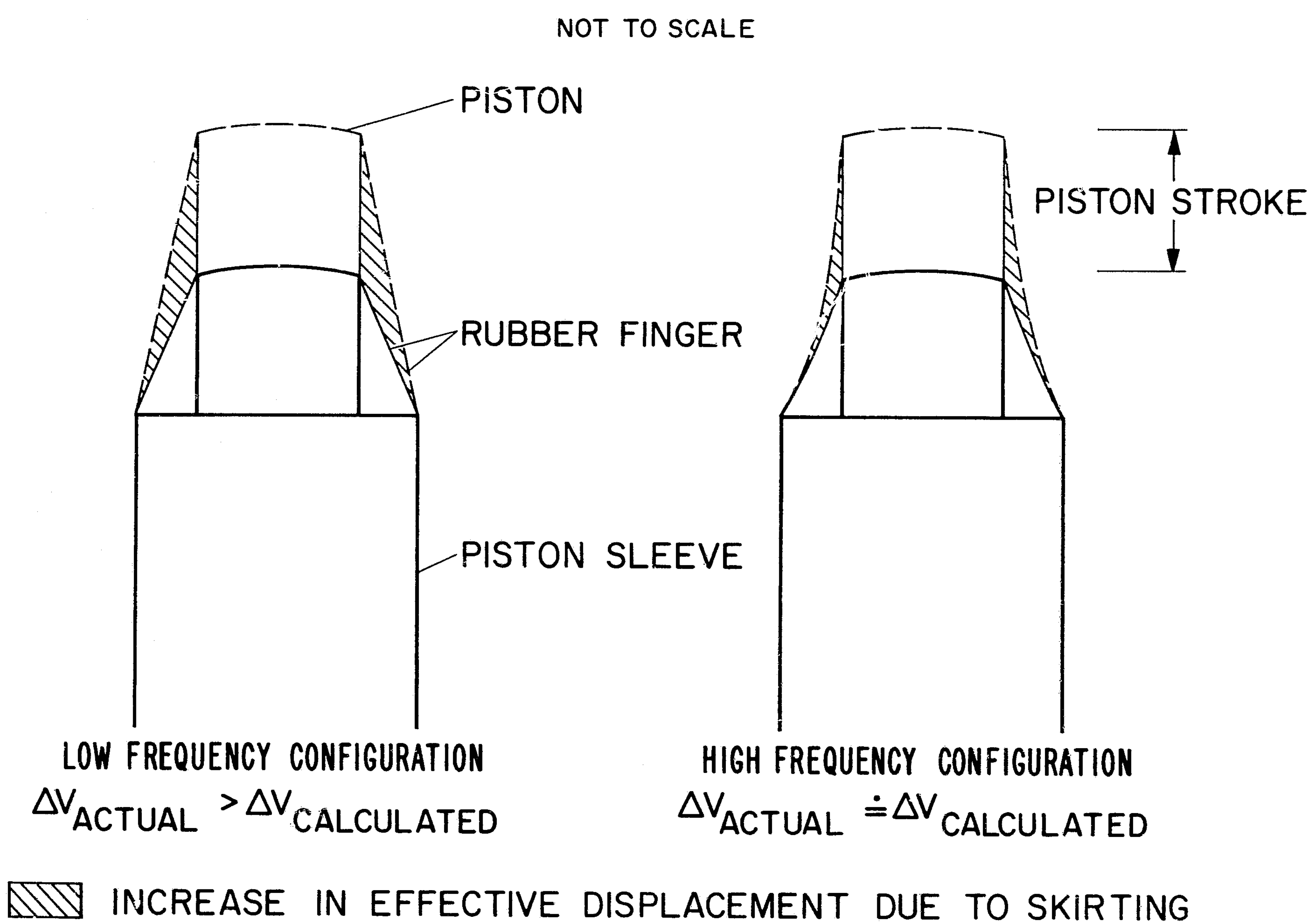

Figure 14. Effect of Skirting Phenomenon on Piston Displacement

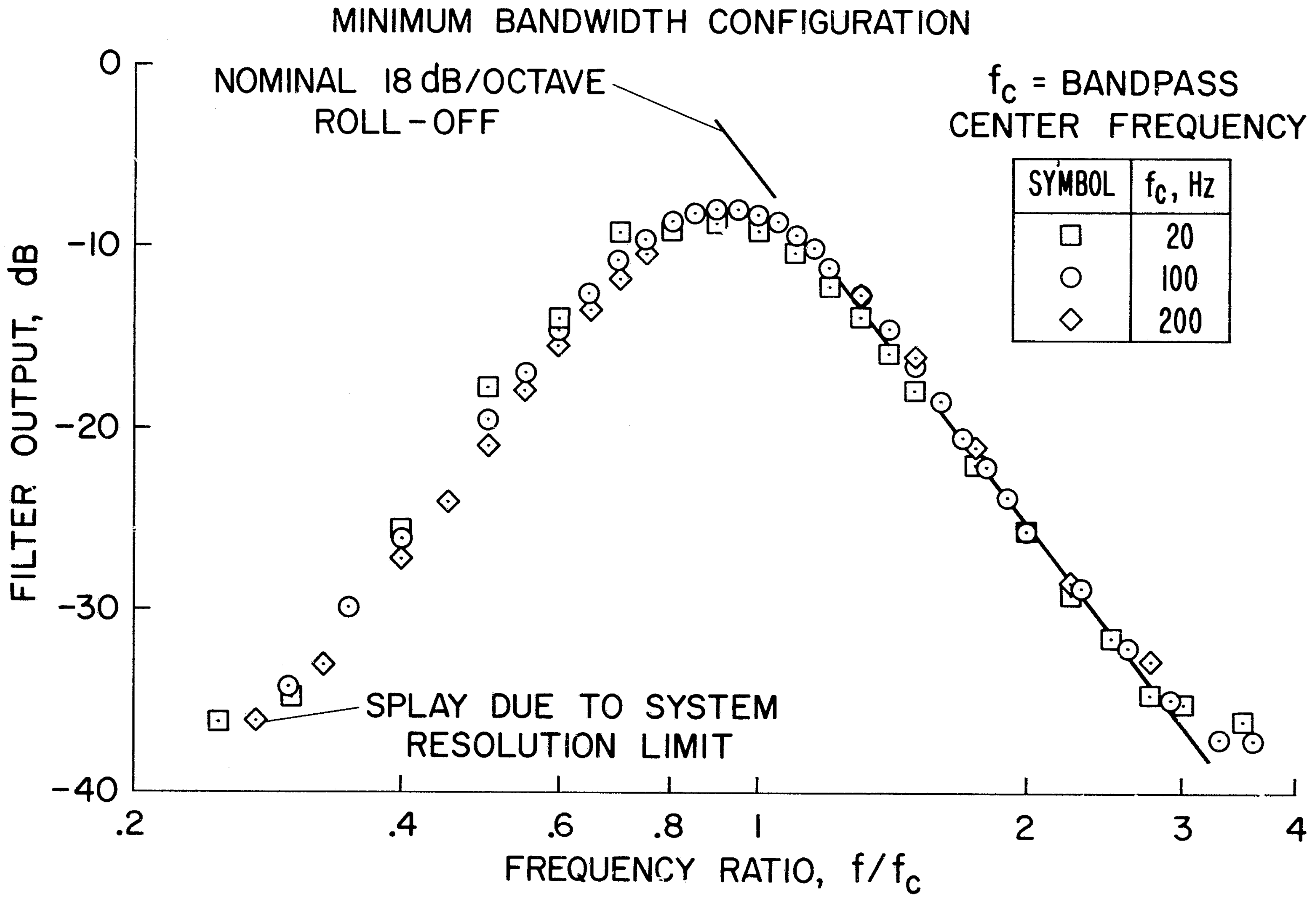

Figure 15. Calibration of Krohn-Hite Model 330M Variable Band-Pass Filter

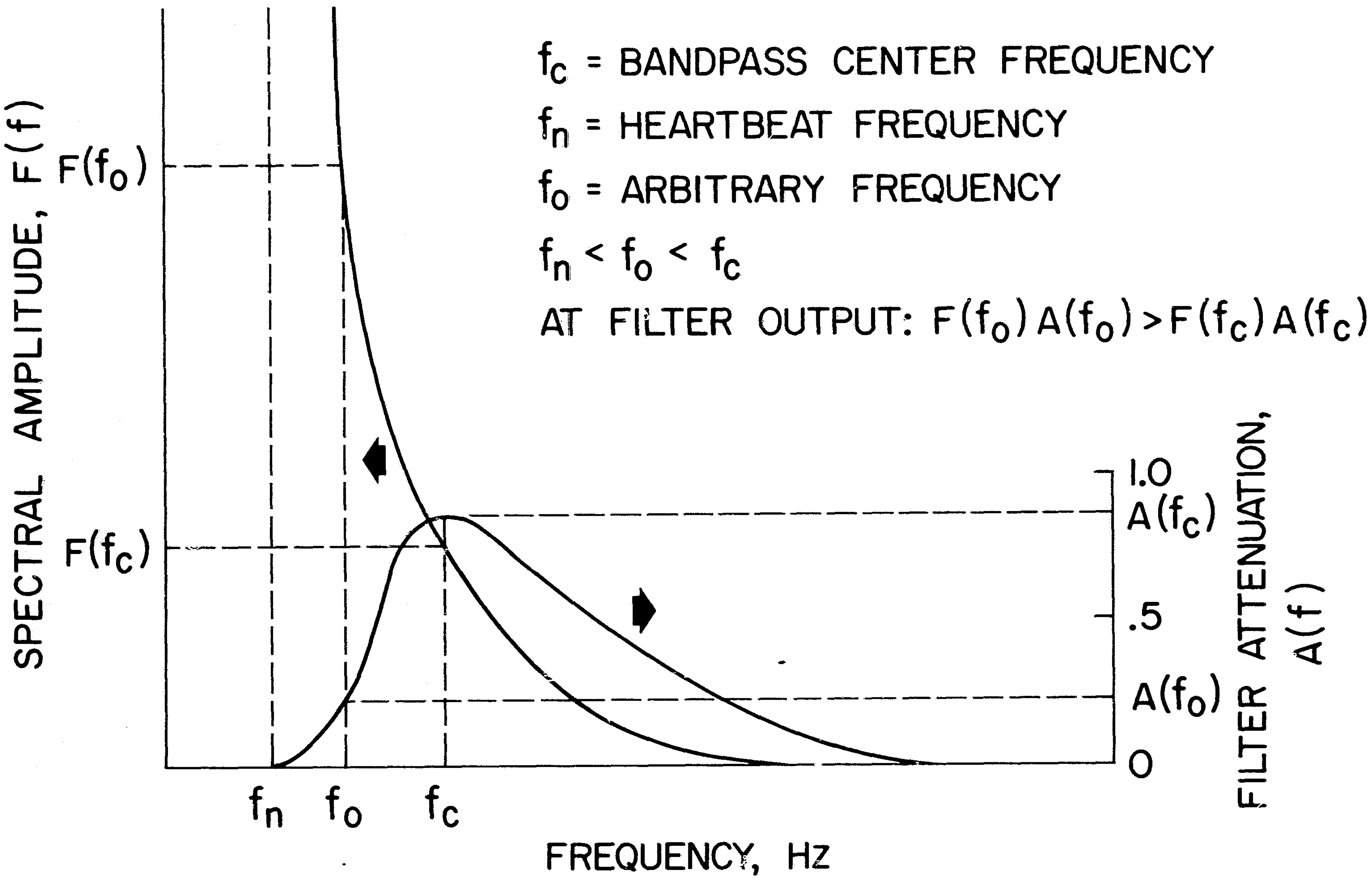

Figure 16. Schematic Illustration of the Effect of Filter Roll-Off on Filter Output When Operating Within the Fourier Spectrum of the Ventricular Pressure Profile

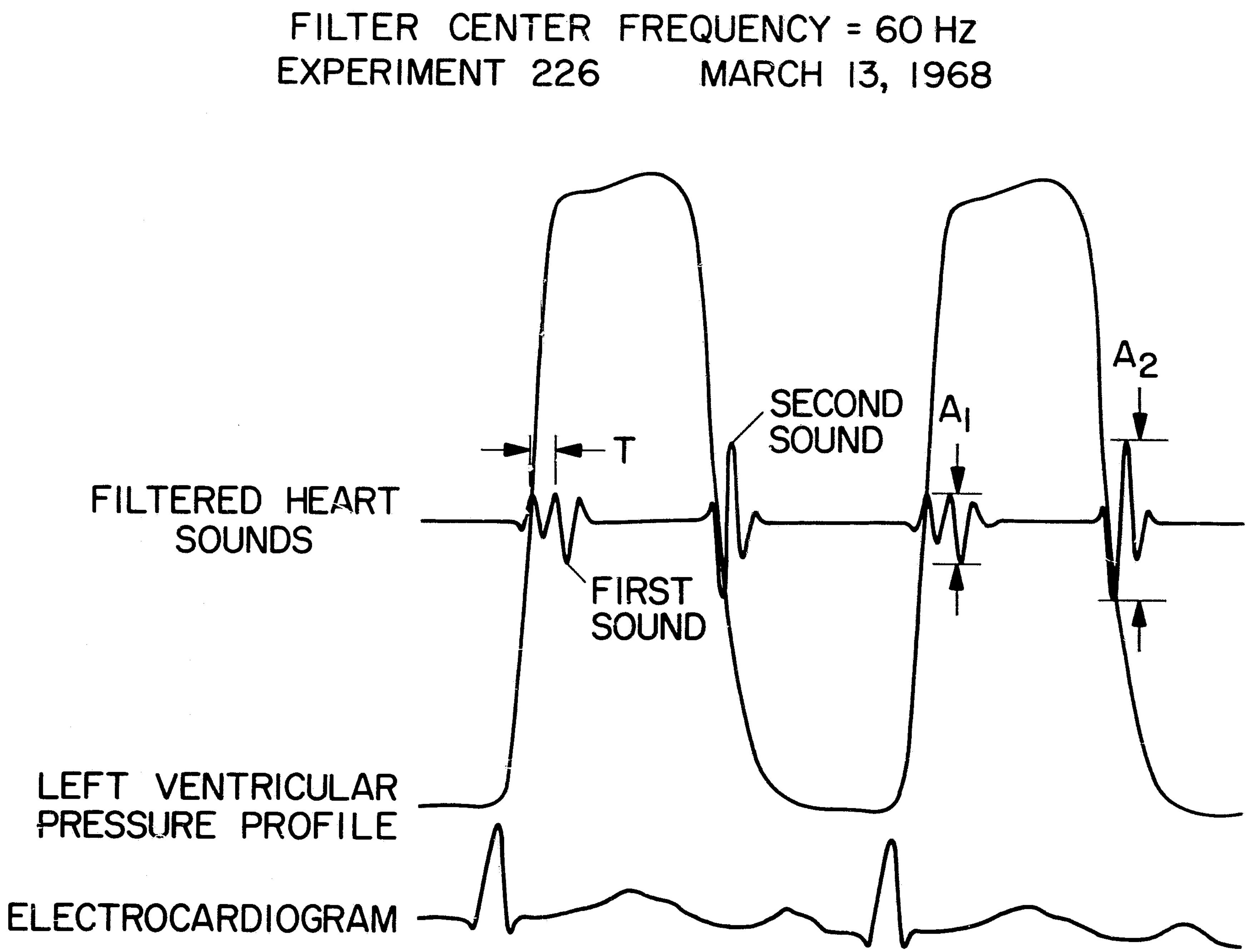

Figure 17. Recordings of Filtered Natural Heart Sounds From the Left Ventricle

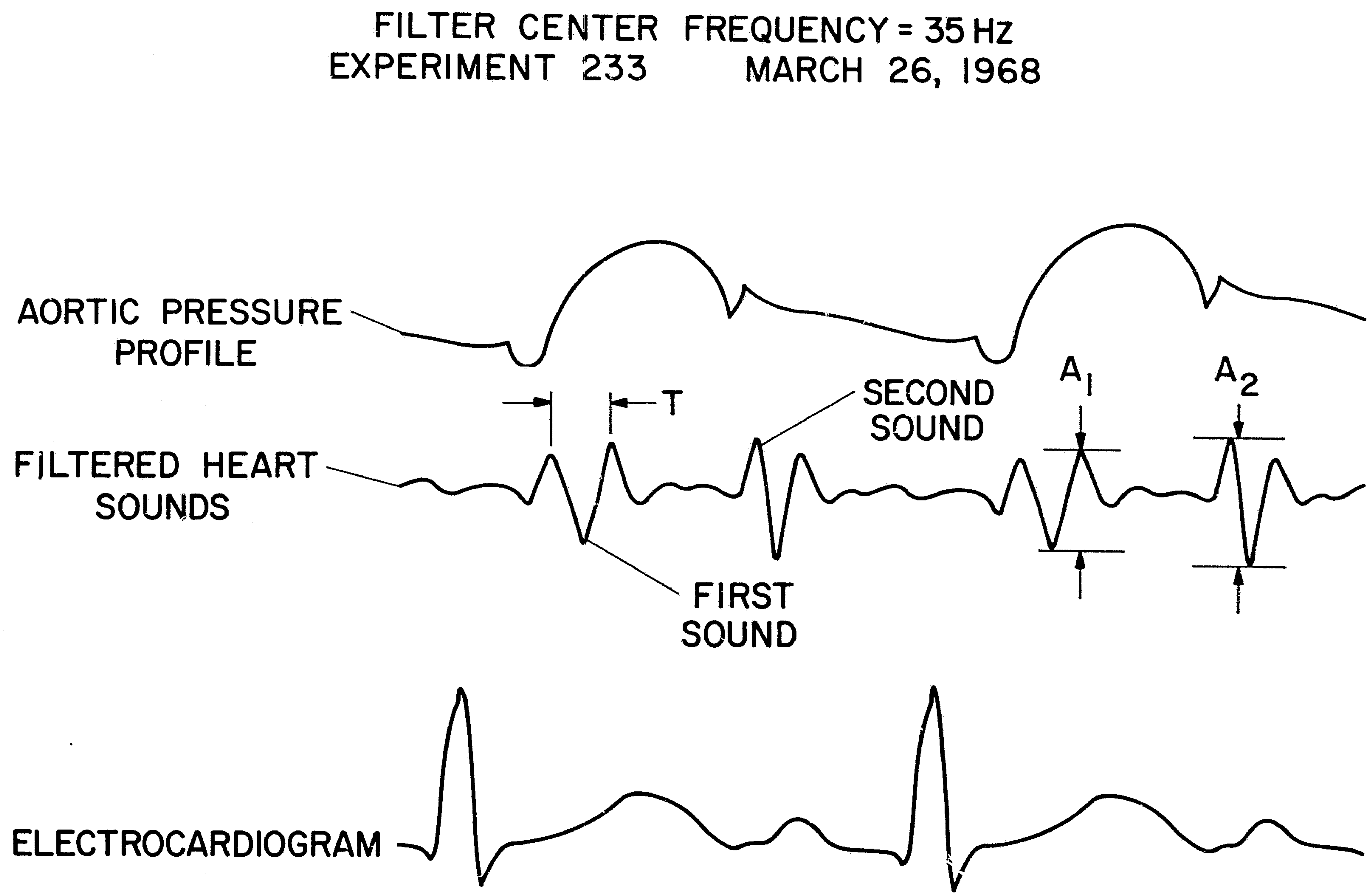

Figure 18. Recordings of Filtered Natural Heart Sounds From the Ascending Aorta

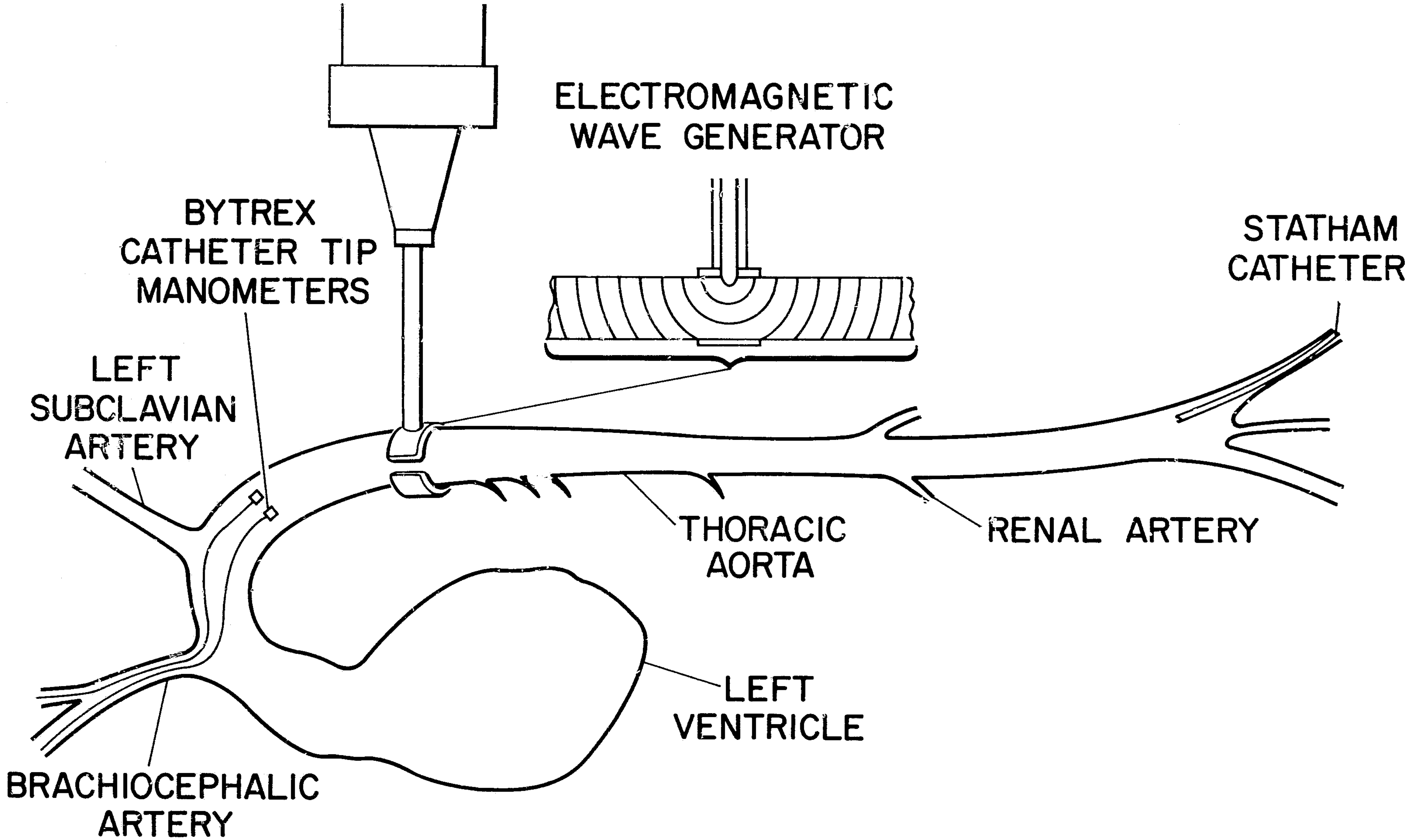

Figure 19. Schematic Illustration of the Experimental Arrangement for Calibration of the Heart Sound Transducer, Filter and Recording System

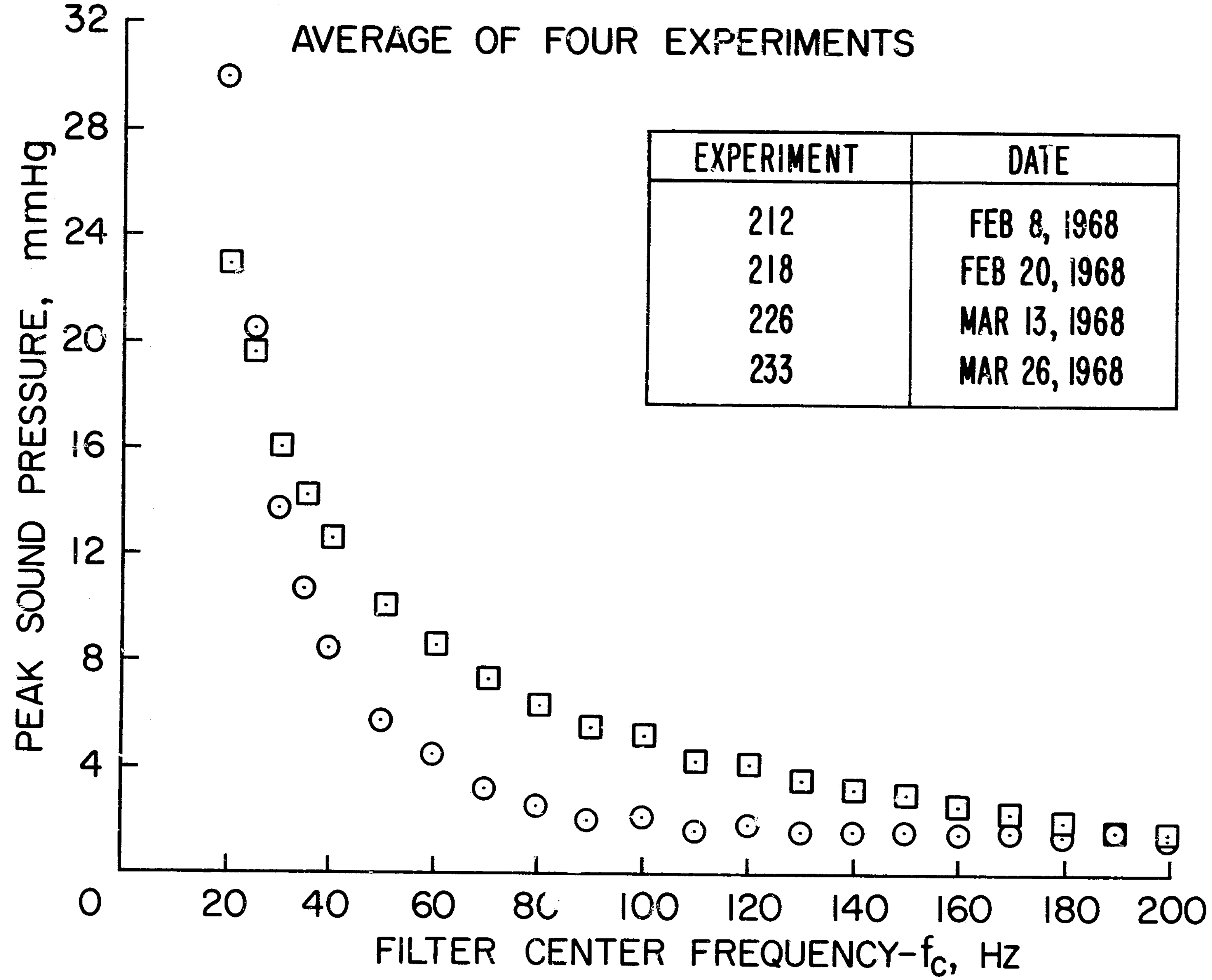

Figure 20. Uncorrected First and Second Heart Sound Spectra Recorded in the Left Ventricle

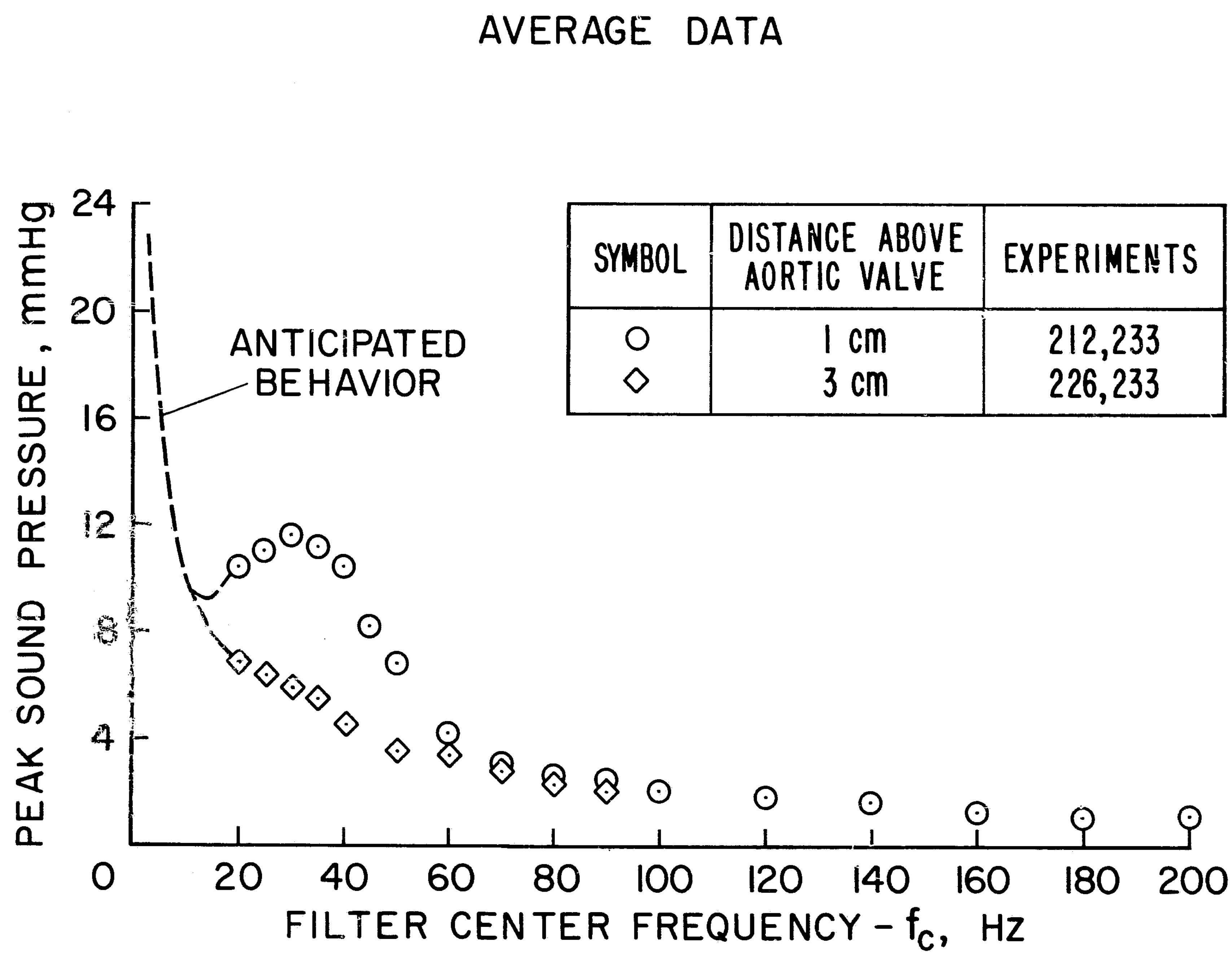

Figure 21. Uncorrected First Heart Sound Spectrum Recorded in the Ascending Aorta

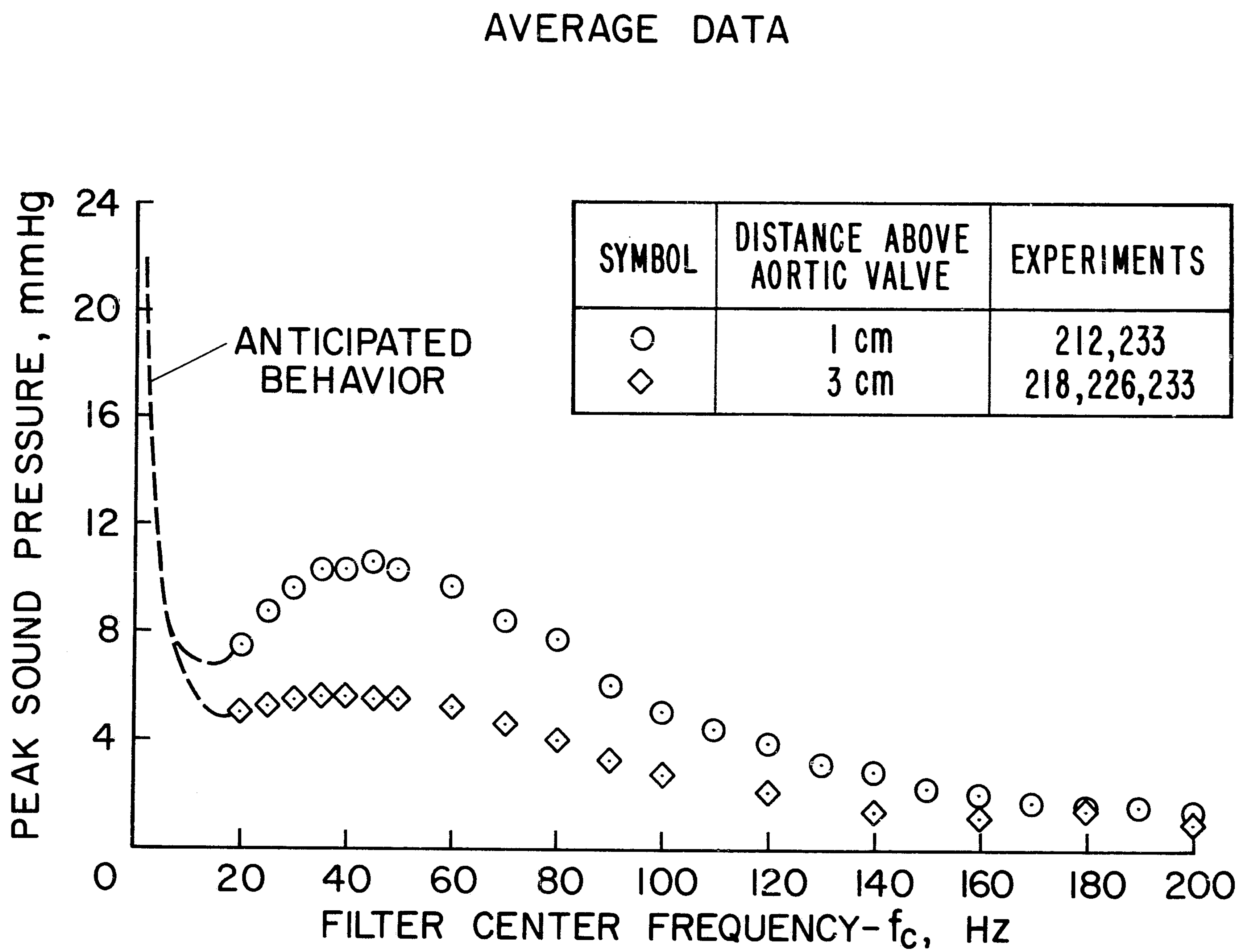

Figure 22. Uncorrected Second Heart Sound Spectrum Recorded in the Ascending Aorta

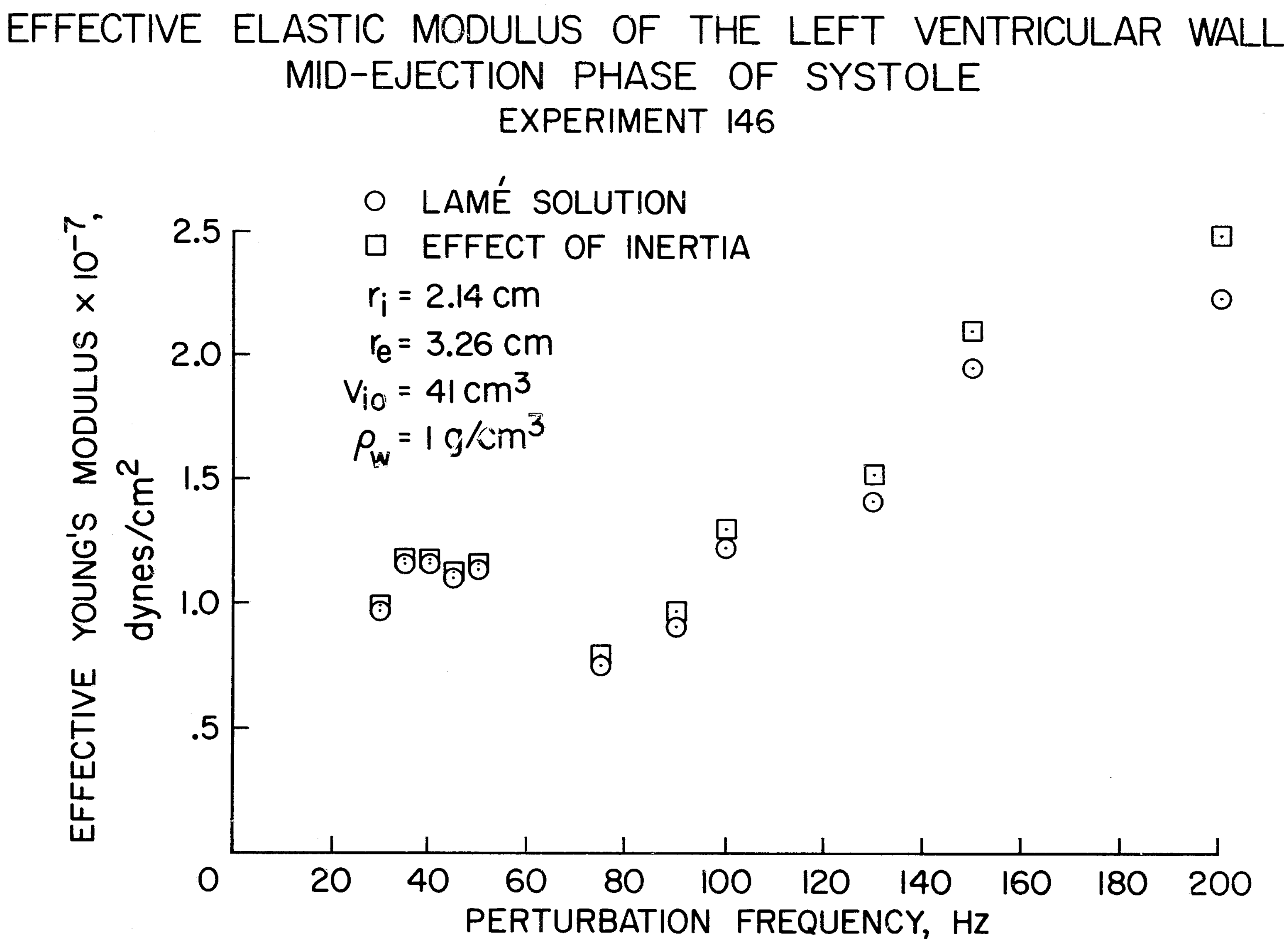

Figure 23. Variation of Effective Elastic Modulus of the Left Ventricular Wall With Frequency, Experiment 146

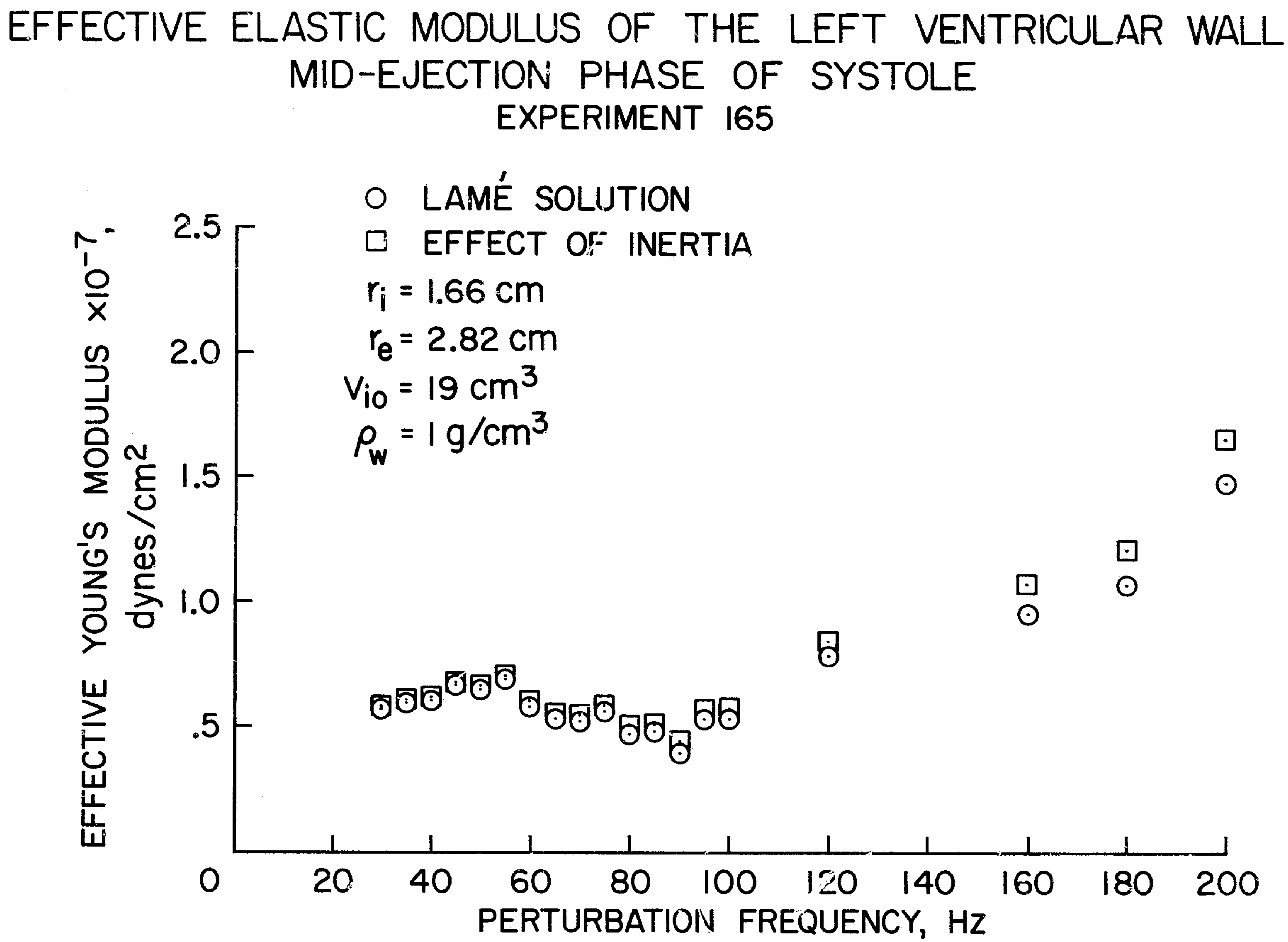

Figure 24. Variation of Effective Elastic Modulus of the Left Ventricular Wall With Frequency, Experiment 165

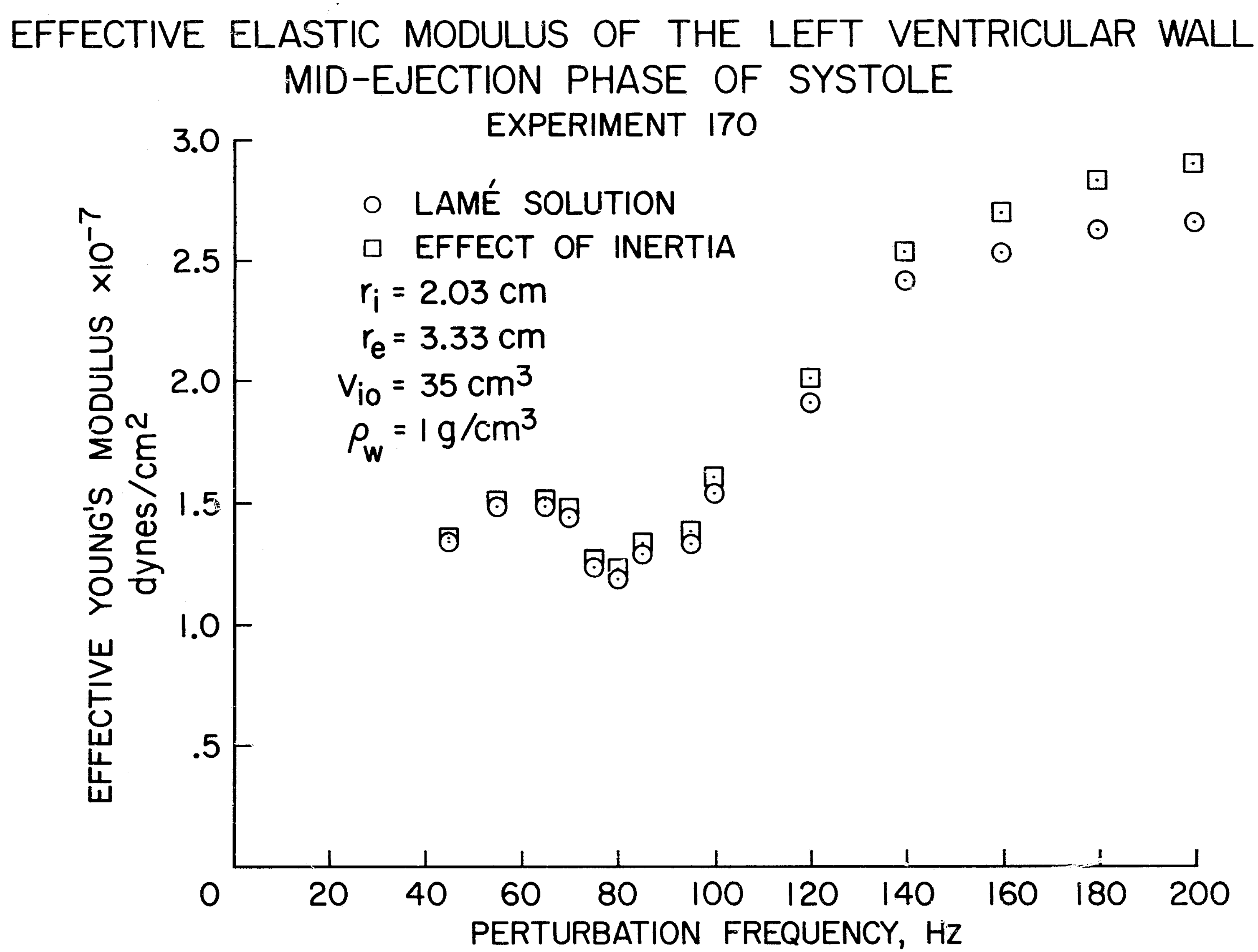

Figure 25. Variation of Effective Elastic Modulus of the Left Ventricular Wall With Frequency, Experiment 170

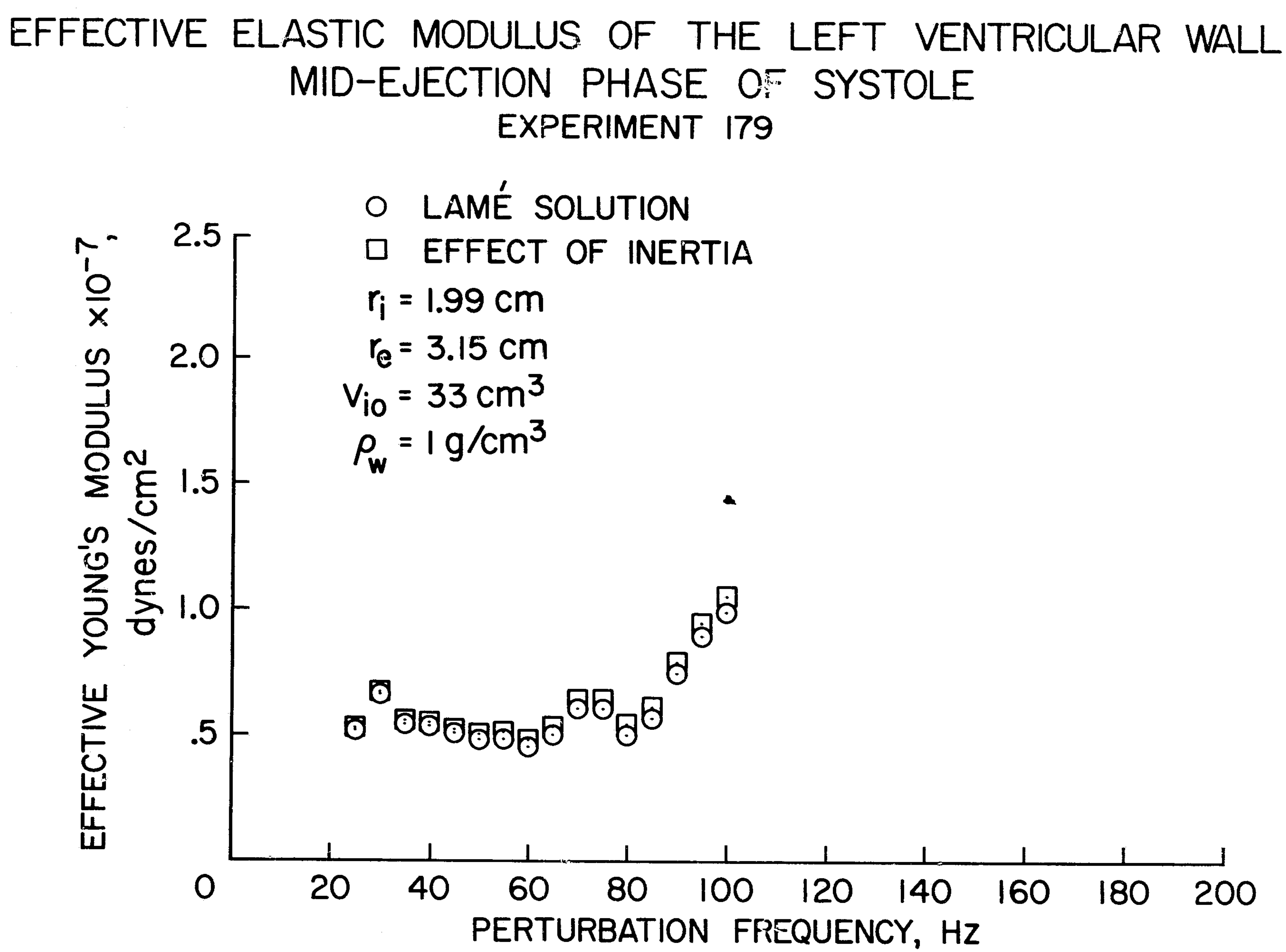

Figure 26. Variation of Effective Elastic Modulus of the Left Ventricular Wall With Frequency, Experiment 179